END

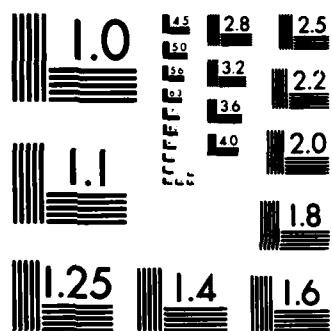FILMED

MICROCOPY RESOLUTION TEST CHART

NATIONAL BUREAU OF STANDARDS-1963-A

AD-A148 960

(12)

ADVANCED ARTIFICIAL DIELECTRIC MATERIALS FOR MILLIMETER WAVELENGTH APPLICATIONS

Annual Technical Report

Contract No. N00014-83-C-0447

ISRAEL S. JACOBS

General Electric Company
Corporate Research and Development
P.O. Box 8
Schenectady, NY 12301

26 October 1984

Report Period 1 Aug. 1983 - 30 Sept. 1984

Prepared for:

Office of Naval Research
800 North Quincy St.
Arlington, Virginia 22217

DTIC
ELECTE
JAN 7 1985
S
D
B

THIS FILE COPY

84 11 21 06 6

REPORT DOCUMENTATION PAGE

1a. REPORT SECURITY CLASSIFICATION UNCLASSIFIED	1b. RESTRICTIVE MARKINGS
2a. SECURITY CLASSIFICATION AUTHORITY	3. DISTRIBUTION/AVAILABILITY OF REPORT
2b. DECLASSIFICATION/DOWNGRADING SCHEDULE	**DISTRIBUTION STATEMENT A** Report ~~for any purpose by the~~ Unit **Approved for public release** **Distribution Unlimited**
4. PERFORMING ORGANIZATION REPORT NUMBER(S)	5. MONITORING ORGANIZATION REPORT NUMBER(S)

6a. NAME OF PERFORMING ORGANIZATION General Electric Company Corporate Research & Development	6b. OFFICE SYMBOL (If applicable)	7a. NAME OF MONITORING ORGANIZATION Office of Naval Research Code 430
6c. ADDRESS (City, State and ZIP Code) P.O. Box 8 Schenectady, NY 12301		7b. ADDRESS (City, State and ZIP Code) 800 North Quincy St. Arlington, VA, 22217

8a. NAME OF FUNDING/SPONSORING ORGANIZATION	8b. OFFICE SYMBOL (If applicable)	9. PROCUREMENT INSTRUMENT IDENTIFICATION NUMBER N00014-83-C-0447

8c. ADDRESS City, State and ZIP Code	10. SOURCE OF FUNDING NOS.			
	PROGRAM ELEMENT NO.	PROJECT NO.	TASK NO.	WORK UNIT NO.
	61153N	RR02202	OC	

11. TITLE (Include Security Classification) ADVANCED ARTIFICIAL DIELECTRICAL MATERIALS (U)

12. PERSONAL AUTHOR(S) I.S. Jacobs

13a. TYPE OF REPORT Annual Report	13b. TIME COVERED FROM 83Aug01 TO 84Sep30	14. DATE OF REPORT (Yr., Mo., Day) 84 Oct 26	15. PAGE COUNT 47

16. SUPPLEMENTARY NOTATION

Full title of contract: Advanced Artificial-Dielectric Materials for Millimeter Wavelength Applications (U)

17	COSATI CODES		18. SUBJECT TERMS (Continue on reverse if necessary and identify by block number)
FIELD	GROUP	SUB. GR.	Artificial Dielectrics, Induced Magnetic Permeability, Properties of Heterogeneous Media, Fine Powder Preparation Techniques

19. ABSTRACT (Continue on reverse if necessary and identify by block number)

An artificial dielectric polymeric composite containing alloy particles which are oxide-coated for isolation and ferromagnetic below room temperature for packing determination, is described. Induced magnetic dipole effects are calculated and compared with measurements of complex permeability in the centimeter wavelength range. Dielectric behavior, according to various theoretical model of heterogeneous media, is explored and correlated to experimental systems. Evidence of higher-order multipole effects and packing-limit effects in random composites is presented. Several advanced preparation techniques for fine powder were initiated.

20. DISTRIBUTION/AVAILABILITY OF ABSTRACT UNCLASSIFIED/UNLIMITED ☐ SAME AS RPT ☐ DTIC USERS ☒	21. ABSTRACT SECURITY CLASSIFICATION UNCLASSIFIED	
22a. NAME OF RESPONSIBLE INDIVIDUAL W.R. Schmidt, CDR, USN (ONR)	22b. TELEPHONE NUMBER (Include Area Code) 202/ 696-4408	22c. OFFICE SYMBOL Code 430B

DD FORM 1473, 83 APR EDITION OF 1 JAN 73 IS OBSOLETE.

TABLE OF CONTENTS

LIST OF ILLUSTRATIONS

LIST OF TABLES

PREFACE

This report was prepared by General Electric Corporate Research and Development under ONR Contract No. N00014-83-C-0447. The Principal Investigator was Dr. Israel S. Jacobs of the Electronics Materials Program, Device and Display Branch, VLSI Technology Laboratory.

The program was administered under the direction of CDR William R. Schmidt, USN, Code 430B, of the Office of Naval Research, Arlington, VA, 22217.

DTIC
ELECTE
JAN 7 1985
S   D
B

RE: Classified Reference, Distribution
Unlimted
No change per Cdr. W. R. Schmidt, ONR/Code
430B

Accession For
NTIS CRA&I
DTIC
Un

Ju

PER LETTER

By
Dist

Av

Dist

A-1

SUMMARY

The development of an interesting artificial dielectric is described. The metallic alloy particles ($Ni_{92}Cr_8$) are oxide-coated for isolation and ferromagnetic below a Curie point of 165K to facilitate determination of volume loading in the composite. Particle size as well as volume loading are significant factors in the electromagnetic properties of the composites. Induced magnetic dipole (eddy current) effects depend markedly on the ratio of particle radius to skin depth which in turn depends on frequency and resistivity. The material and measurement parameters of this study span the range of interesting behavior. Measurements of the complex permeability agree satisfactorily with calculations. These phenomena have technological implications for real systems in extremes of frequency and/or temperature. An up-to-date exploration of theoretical descriptions of the dielectric properties of heterogeneous media was made. They successfully account for the relatively simple Maxwell (Maxwell-Garnett, Clausius and Mossotti) behavior observed for artificial dielectrics of the present class. The effects of higher-order multipole interactions and geometrical packing limits calculated for regular lattice arrays are found in the random composites, with deviations that may reflect details of the composite microstructure.

Work was also initiated on alternative passivation coatings and on the preparation of very fine powders by the spark erosion method. Such powders are intended for an empirical optimization of metallic magneto-dielectric composite systems in the centimeter wavelength range. The spark erosion method presents several potential advantages of technological interest.

I. INTRODUCTION

This research is concerned with the development of a novel class of artificial dielectrics and a deeper understanding of its properties at millimeter wavelengths. Our starting point is the "Theoretical Radar Absorbing Materials Physics Model" developed during a classified program [1]. That study involved experiment and analysis of a broad data base obtained from measurements in the microwave range of frequencies (centimeter wavelengths). Many of the model features and predictions are, however, relevant to the millimeter wavelength region. Some of the more interesting implications of the work concern the dielectric property behavior of the composite system, one which may be regarded as a new class of oxide-passivated metal-insulator dielectrics.

An overview of the research goals for the current three-year study may be stated in question form as follows: How valid is the RAM Physics Model in higher frequency regimes? Why does the dielectric behavior follow the simple Maxwell approximation, given the pitfalls that often beset metal-insulator composites? Has the artificial (magneto-)dielectric system been optimized in the centimeter wavelength regime? Can composites be fabricated which work well in the millimeter wavelength regime? How do they compare with other materials approaches?

Alternatively, a more formal view of the program can be adopted from the Statement of Work given in the proposal. We reproduce as Table 1 the program schedule with time lines revised to fit the investigator's calendar, i.e., the contract start date is 1 Aug 83 but formal signing and notification did not occur until about mid-September 1983. At an oral review/site visit by the ONR Scientific Officer on 12 June 1984, some task revisions were discussed and tentatively approved. These involved expansion of effort in Tasks 1 and 3, balanced by removal of Task 4. The rationale for these changes is developed herein.

TABLE 1

PROGRAM SCHEDULE
AT START OF CONTRACT

Task	CY '83	CY '84	CY '85	CY '86
1. Investigate Effect of Binder Permittivity in Artificial Dielectrics.	•• ───────────△			
2. Analyze Effects of Microstructure Control in Passivated Metal Insulator Composites.	•• ──────△			
3. Develop Alternative Theoretical Approaches to Composite Dielectrics.	──────△			
4. Search for Percolation Transition: Exploitation and Control.	───────────△			
5. Explore Alternative Passivation Coatings/ Investigate High Frequency Properties.	──────────△			
6. Quantify Skin-Depth Effects in Passivated Artificial Dielectrics.	───────────────△			
7. Investigate Millimeter-Wavelength Properties of Artificial Dielectric Composites.	─────────△			
8. Investigate or Simulate Temperature Dependence of High Frequency Properties.	─────────△			
9. Reporting — Annually and Final	△ △ △			

1

II. TASKS 1, 2, and 3

The concurrent work on these three tasks during the reporting period has been so mutually interactive that it is better to consider their methods and results more or less together. The presentation of the segments will skip among the numbered Tasks in order to demonstrate a purposeful course.

II.1 Development of an Artificial Dielectric

With initial emphasis of the program on the dielectric aspects, an important phase has been the development of a suitable laboratory artificial dielectric. The model idea of a dielectric which consists of a series of metallic globules separated from each other by insulating material goes back at least to Faraday in 1837. An excellent history of inhomogeneous media concepts has been recorded by Landauer [2].

II.1.1 Criteria

Our criteria are that the metal (alloy) powder be non-magnetic at room temperature but ferromagnetic at low temperature to facilitate determination of the volume loading, p. The latter quantity is key to quantifying the dielectric behavior. We also require that the powder be capable of developing a thin *insulating* oxide layer on each particle. We contrast this with some other work in which researchers have encouraged formation of a thin oxide coating in powder preparation to discourage initial agglomeration but kept it thin enough to allow metal-to-metal contact between the particles under sufficient pressure [3].

The choice of candidate alloys thus involved magnetic and metallurgical consideration. Added to these is the challenge of fine metal powder preparation. For this task area we made use of our gas-atomization facilities. In this process [4] molten alloy is forced through a specially designed nozzle and the liquid stream is disrupted by high velocity gas blasts to create fine droplets. These solidify as they descend in a large volume settling chamber. In one of our facilities liquid substrate quenching is a special feature, i.e., a blast of water spray follows the gas jets.

II.1.2 Consideration of Candidate Metallic Systems

Desirable alloy systems were therefore such that one of the elemental components would tend to form a stable and at least partially protective oxide. Some usual examples of this category are Al, Cr and Y. Folding these in with the magnetic considerations, yielded several suggestions, e.g., Ni with Cr, Gd with Y, and (Cu-Ni) with Al. The first two systems are reasonably well known magnetically in handbooks [5] or in more recent [6] research while the third has had little exploration [7]. The Gd-Y combination was quickly rejected (by our metallurgical colleagues) as explosively undesirable. Although the solubility of Al in the Ni-Cu host is modest, at about 10 at % ($\sim$5 wt %), there appeared to be a fair prospect of a Curie point below room temperature. We chose to prepare an exploratory ingot with the composition (by weight) Ni90Cu5Al5. Finally for Ni-Cr, the wide range of solubility and well-known magnetic properties enabled us to specify "with confidence" an ingot composition of Ni92Cr8 with every expection of a Curie point near 240K, and a low temperature saturation magnetization of about $\sigma_\infty(0°K) = 21.8$ emu/g.

II.1.3 Magnetic Characterization of Candidate Metallic Systems

Thermomagnetic scans, magnetization vs. temperature at 50 Oe, along with low temperature (6K, 20K) saturation magnetization data, were measured. For this purpose we have a vibrating sample magnetometer system with capabilities from 4K to 1370K ($\sim$1000C) and fields up to 25kOe. The scans are shown in Figure 1. As for the Ni-Cu-Al ternary, its T_c centered at 256K but there was a risk of some residual undesirable ferromagnetism at room temperature. The opposite problem presented itself with Ni92Cr8. Both the Curie point and the magnetization fell short of confident expectations by a factor of 2! In searching for the "fault" here, we verified the chemical composition of the ingot, and also prepared a second ingot with composition Ni94Cr6. Its T_c, measured as 237K, again compares poorly with the literature value of 335K! At this point we were facing an unexpected, annoying and delaying problem. A resolution of the dilemma was clearly warranted because this Ni-Cr system remained the most attractive of the ones considered as candidates.
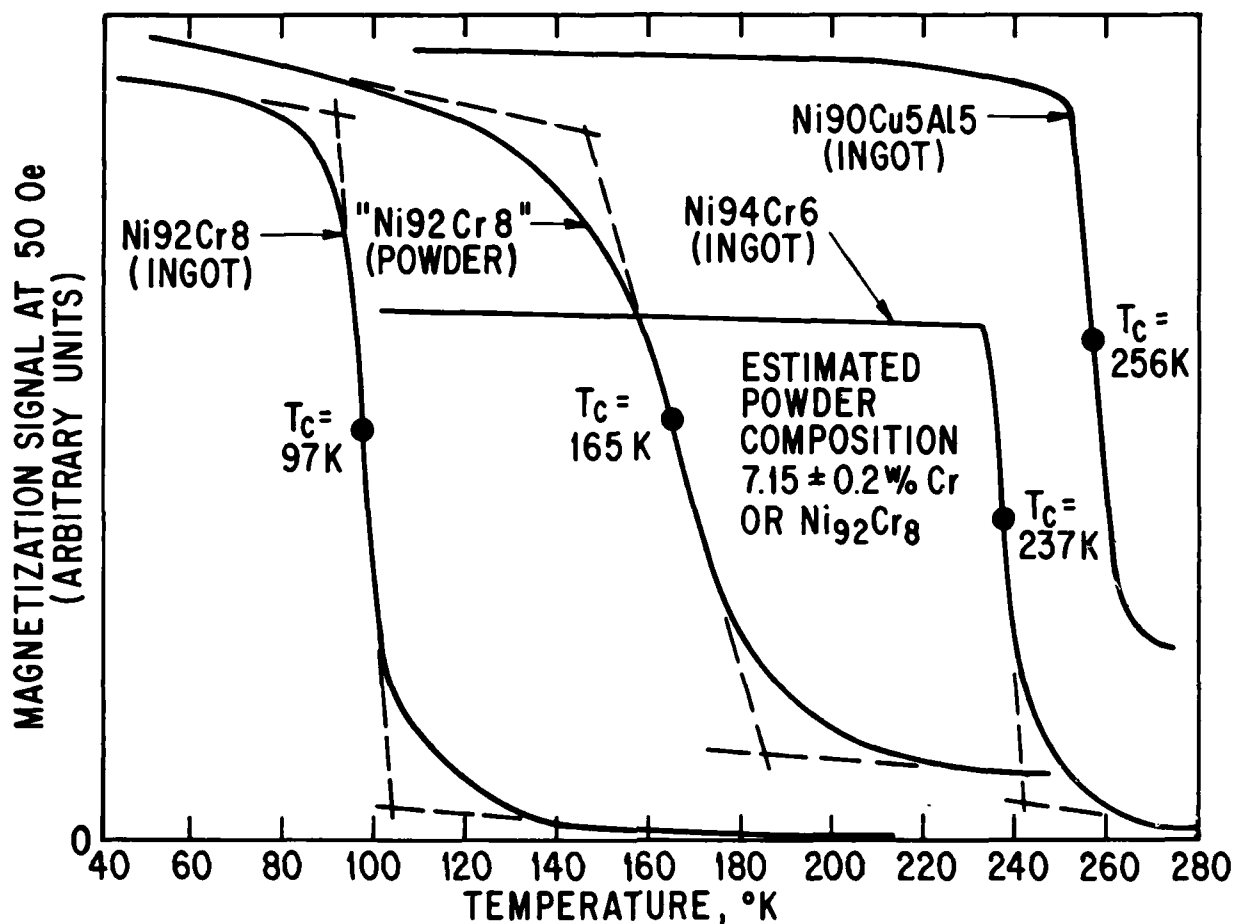
Figure 1. Thermomagnetic analysis of candidate alloys and atomized powder.

II.1.3.1 Exploration of Magnetic Characterization Problems

The solution of the problem and the "validation" of our own work came from a detailed look at the published literature both backward from the handbook data and forward to the present time via a library bibliographic search. The magnetic measurements cited in the standard References [5] are based on experimental work from the Strasbourg laboratory directed by P. Weiss, a world-famous organization that set most of the standards for current magnetics research. In studying the primary sources, the research of Marian [8] and Sadron [9], it emerges that they used identical alloy samples which had been prepared earlier by Šafránek [10], also at Strasbourg. In the preparation, he had been concerned with the purity of the available starting materials, especially the chromium. Indeed, he ultimately prepared his own Cr by an electrolytic process, to combine with high purity Mond nickel. Satisfactory metallurgical micrographs were shown, indicating single phase alloys. Inasmuch as our Curie points are markedly lower, a suspicious investigator may still want to raise the purity question. How much residual Fe or Co in either component would be needed to shift the results into "accord"? More tolerance is in order with regard to the magnetic saturation because the French workers had to extrapolate downward from 110K toward absolute zero. However, their results are 40% to 100% greater than ours!

As one looks forward from the standard references into the most recent two decades, a different picture emerges. A group at Leiden [11] in 1962 noticed some differences in saturation magnetization for alloys of 5.6 at % and 9.1 at %, and in an estimate of T_c for the former alloy, but politely called these

3

"small discrepancies." Next, a rather thorough investigation in 1972, at Strasbourg by Besnus et al., [12] (on newly prepared samples and including low-temperatures) presented results which differed quite a bit from the early data though not quite as much as the Leiden results. They diplomatically omit to mention that they differ from their colleagues of an earlier generation! The emerging picture is displayed in Figure 2 for Curie points and in Figure 3 for saturation magnetization. (Compositions are in atom percent, as used by these research workers. In the region of interest to us, i.e., 6-8 wt%, the amount in atom % is about one integer higher). More recently a study from Japan [13] gave results in close agreement with Besnus et al., and did make a significant graphical display of the differences with the early work. Lastly, Simpson and Smith in 1982 report [14] especially on compositions with quite low Curie points, in close agreement with our measurements.

While examination of the comparative results in Figures 2 and 3 does not fully settle the question of which set is correct, the existence of a major discrepancy with the early work is established. The present work on the several ingots sets the base line for subsequent magnetic evaluation of powder properties and ultimately, for our original goal, of volume loadings in artificial dielectric composites.
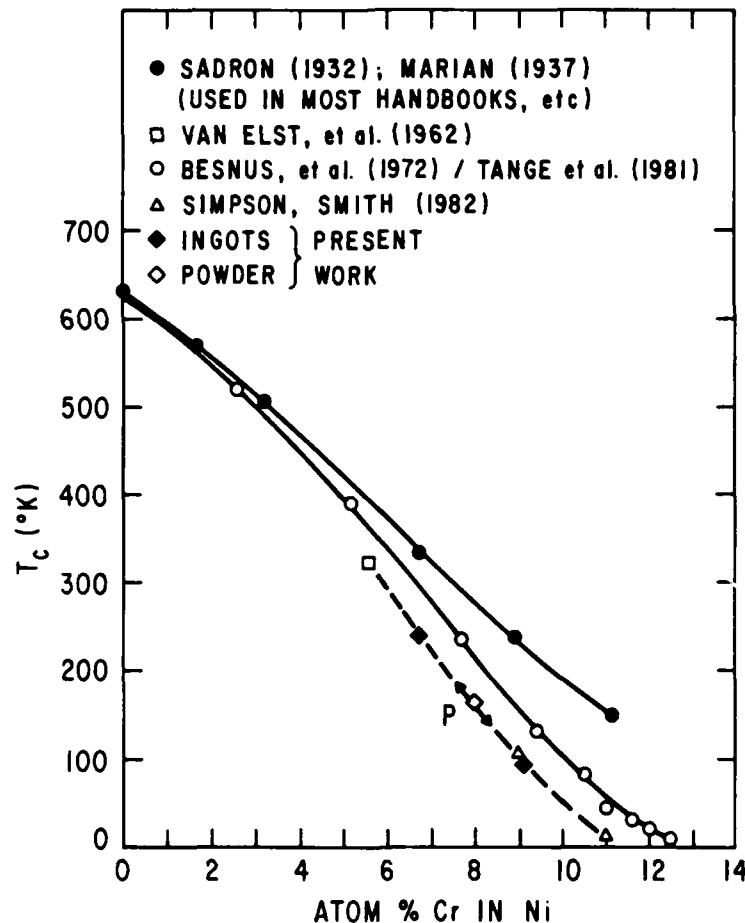
Figure 2. Ferromagnetic Curie points as a function of composition in Ni-Cr solid solution alloys including work of other investigators as well as present results.

4
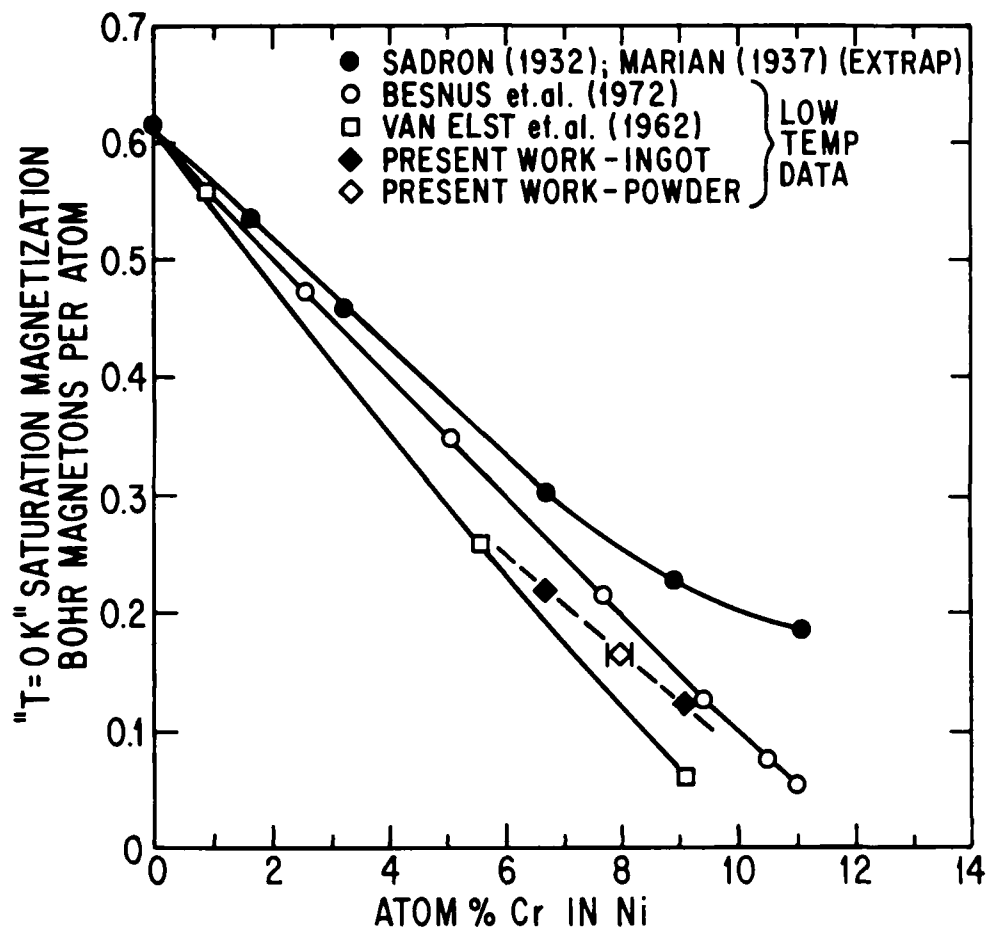
Figure 3. Saturation magnetization per average atom vs. composition for Ni-Cr alloys including available literature data.

II.1.4 Preparation and Magnetic Characterization of Metal Powder

At this stage we were ready for powder preparation. We anticipated (correctly) that there would be some composition shift in this step toward a higher Curie point and thus we selected the ingot Ni92Cr8 (about 9 at. % Cr) in order to keep the alloy non-magnetic at room temperature.

Two atomization trials of the Ni92-Cr8 alloy were performed. In both cases the melt was atomized while at a temperature of 1870K by argon gas at 4.28 MPa. The high melt temperature was employed to reduce the melt surface tension and melt viscosity while the high gas pressure resulted in a high gas jet velocity. (Mach Number ≈3.2). Previous analysis has shown that fine powder sizes are favored by increased gas velocity and decreased melt surface tension and melt viscosity.

The two trials were performed using two different versions of the GE-CRD-developed close-coupled gas nozzle. The second run uses an improved form of the close-coupled concept, designed to provide increased yields of fine powder.

The results of the two runs are shown in Figure 4. The particle size distributions between 37μm and 250μm were determined by sieving. The particle size distributions below 37μm were obtained by extrapolation assuming the curves to be log-normal. (This assumption has been verified in other work).
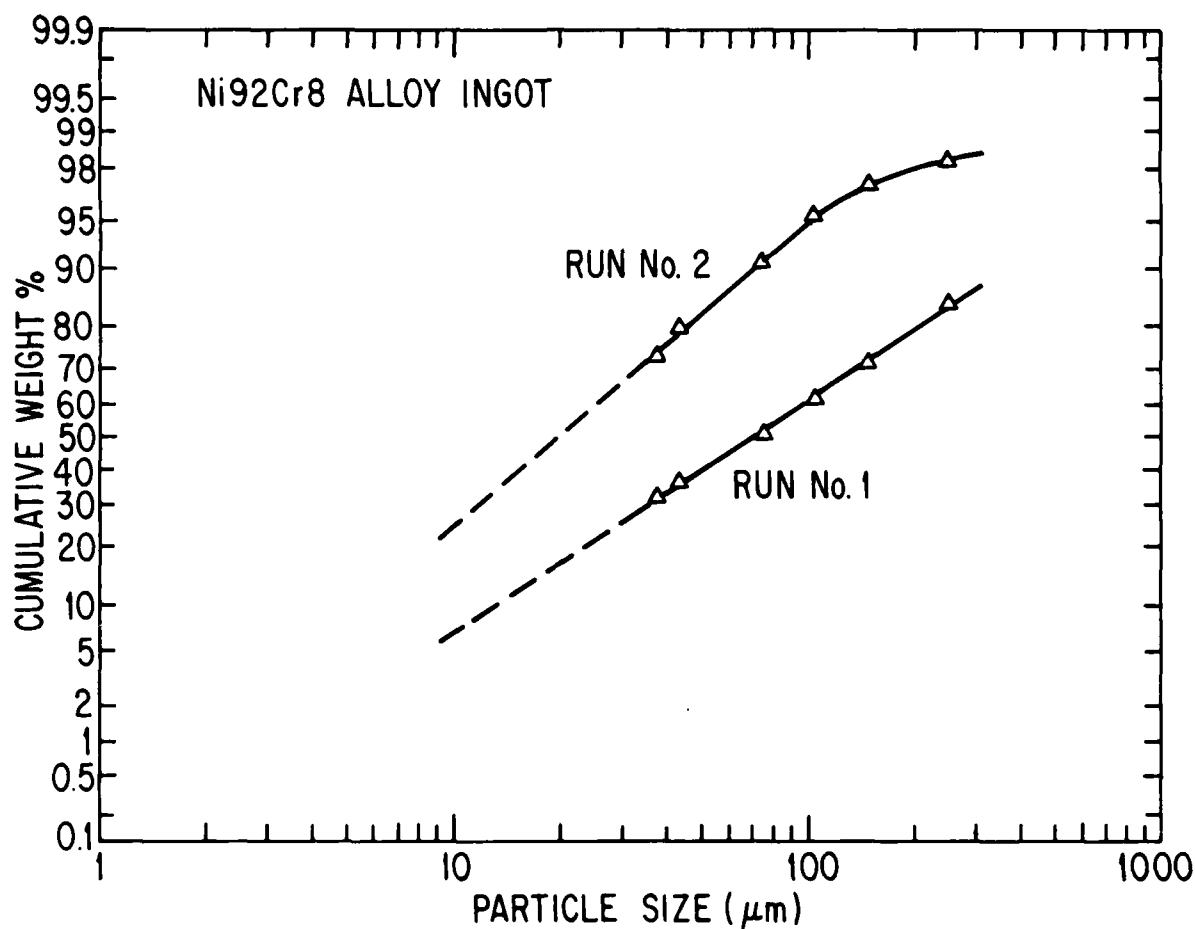
Figure 4. Particle size distributions from 2 gas-atomization runs on Ni92Cr8 alloy.

The thermomagnetic scan of this powder (sieved to $<37\mu m$) is shown in Figure 1. An average Curie point of 165K results, some 68K upward from the ingot. It is broader, suggesting a range of T_c values.

Referring to Figure 2, this T_c translates in composition to about 8 at. %Cr or 7.15± 0.2 wt%Cr. Using this composition, there is satisfactory accord of the saturation magnetization "line" in Figure 3 with the "present work" data.

For the practical record, the magnetization values at low temperature (6K or 20K), extrapolated to infinite field, are 21.2 emu/g and 12.0 emu/g for the ingots Ni94Cr6 and Ni92Cr8 respectively. For the powder we find 16.2 emu/g.

II.1.5 Evaluation of Surface Condition of Metal Powder

The shift in composition during powder preparation corresponds to a net depletion of Cr in the alloy particle. It is tempting to attribute this to an oxide coating of Cr_2O_3. It is much more difficult to examine the surface coating of spherical particles by microprobe techniques, than the surface scales on bulk flat samples. We are, however, attempting to do this on these powder spheres. Conventional oxidation studies on the Ni-Cr system, albeit under isothermal conditions, indicate a moderately complex scaling with NiO, Cr_2O_3, Ni-Cr spinel oxide and other components [15].

6

If we naively (and tentatively) hold to a view that the coating may be Cr_2O_3, we can estimate its thickness from a mass balance. Using a mean diameter of about $23\mu m$ we calculate a shell coating whose thickness is about $0.1\mu m$, which is not unreasonable. A sketch of this rough calculation is as follows:

$$[(w/o\ Cr\ in\ ingot)\ x\ vol.\ sphere\ x\ \rho_{alloy}] =$$

$$= [(w/o\ Cr\ in\ powder)\ x\ vol.\ sphere\ x\ \rho_{alloy}]^+$$

$$+ [(w/o\ Cr\ in\ oxide)\ x\ (vol.\ oxide\ shell)\ x\ \rho_{oxide}),$$

vol. sphere $= 4\pi r^3/3$; vol. shell $= 4\pi r^2\Delta r,$

$$\Delta r \cong \left[\frac{(w/o\ Cr\ in\ ingot - w/o\ Cr\ in\ powder)\ x\ <diam.>\ x\ \rho_{alloy}}{(w/o\ Cr\ in\ oxide)\ x\ 3\ x\ 2\ x\ \rho_{oxide}} \right].$$

We have some results from microprobe techniques on the Ni-Cr powder. As-prepared powder was pressed onto and into an aluminum substrate block for examination by Auger electron spectroscopy. The count rates for the various elements, Ni, Cr and O, were monitored as a function of sputter time. The latter is proportional to depth into the particle being examined, as material is sputtered away. The probe spot used was smaller than the particle diameter (from the powder size fraction $+20, -37\mu m$). Count rates are expressed in atomic percent, after appropriate scaling in the instrument. [Physical Electronics Model 600 Auger Microprobe]. The "depth" probing may not be completely simple because the pressure used in preparing the specimen may have deformed the spherical alloy particle. As an alternative, we hope to obtain a profile on a polished particle as the probe traverses the edge coating.

The depth profile by Auger spectroscopy is shown in Figure 5. While not the simple naive picture we hypothesized, it does have features one might expect. At the surface (t = 0, sputter time) there is a major *build-up* of *oxygen*, from a residual low level representing a sort of background; and a modest, $\sim 50\%$, *build-up* of *chromium* from about 12 at.% to about 18 at .%. Concurrently, there is a major *decrease* of *nickel*, albeit not to the near-zero-level hypothesized. We can attempt to rationalize these data in terms of NiO and Cr_2O_3, there being no evidence for Ni metal in the magnetic data. (Oxidation studies of this system [15] always assume that Cr goes to Cr_2O_3, or more complex spinels or solid solution). The "surface composition," $Ni_{0.32}\ Cr_{0.18}\ O_{0.50}$, is roughly equivalent to $3NiO\cdot1\ Cr_2O_3$, which corresponds to $Ni_{0.27}\ Cr_{0.18}\ O_{0.54}$.

If we oversimplify the surface as a uniform shell (again), we can invoke a mass or atom balance to determine how much material is in the shell. Using the chemically and magnetically determined alloy compositions, we write:

$$Ni_{0.91}\ Cr_{0.09} + 6zO \rightarrow y\ Ni_{0.92}\ Cr_{0.08} + z\ (3NiO\cdot1\ Cr_2O_3).$$
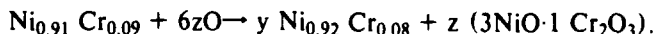
Balance equations for Ni and Cr yield two simultaneous equations in y and z, which are readily solved to yield y = 0.969, z = 0.00625. Approximately 2% of the original nickel goes into the oxide shell, while about 14% of the original chromium makes the transition. This does confirm the general stronger tendency for Cr to oxidize. Expressing the chemical balance in terms of the mass of one average ($23\mu m$) particle and the number of moles of alloy in that particle, we can obtain the masses of NiO and of Cr_2O_3. Converting to volumes (via their separate specific gravity values), and equating their total volume to a "shell" volume, we arrive at the oversimplified thickness of shell of $0.22\mu m$. This is a factor of two greater than the more naive estimate, but it too is only a rough (albeit reasonable) approximation.

II.1.5.1 Resistance Tests of Metal Powder Compacts

As a final *practical* acceptance test for the alloy powder, we attempted to verify that the powder particles were electrically insulated from each other. Conceptually, a check of resistance in powder compacts appears simple. In practice, it is less so. A simple device was constructed consisting of solid copper electrodes which can slide into a plastic cylinder, 1.25 cm inner diameter. We used this with a
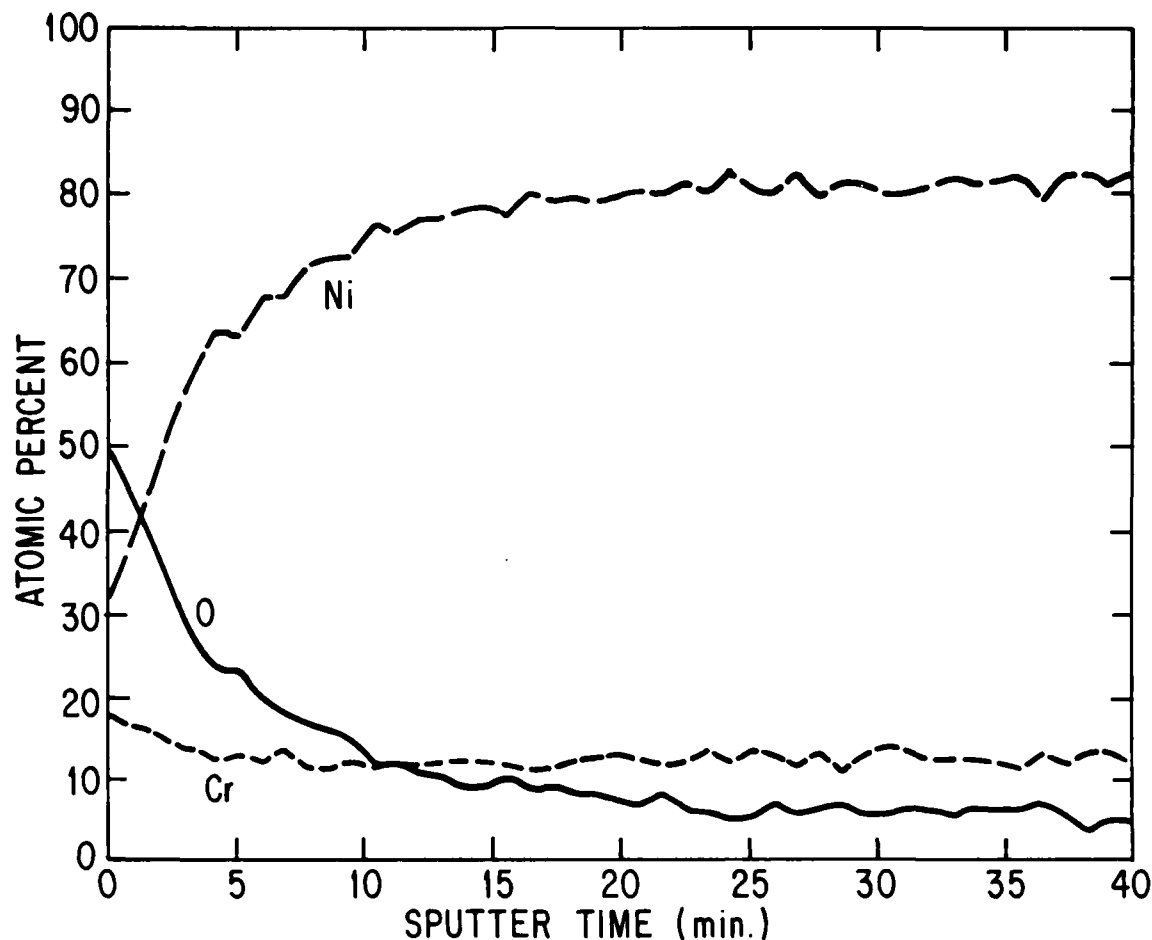
Figure 5. "Depth" profile by Auger electron spectroscopy of Ni-Cr powder compact: Composition vs. sputter time (proportional to depth).

digital multimeter capable of measuring up to 20MΩ resistance. A small amount of alloy powder in the cylinder gave erratic results, dependent on pressure, time, powder column height, etc. Confirmation of this behavior was found in the literature. Ottavi, et al., [16] describe a conceptually elegant experiment to study percolation concepts, i.e., at what composition do continuous electrical paths develop when various mixtures of conducting and insulating spheres are studied? Their experiments were carried out with monodisperse 5mm diameter plastic spheres, a fraction of which had been electroplated with a thin copper coating. It is helpful to quote from their paper, as follows: "In order to obtain stable conductance measurements we find it necessary to apply pressure to the piston bearing the upper electrode. This lack of stability is not that due to fluctuations introduced by the randomness of the mixture. Indeed, even if the system is reduced to only two spheres, the measured resistance is not constant in time, or reproducible between trials, unless a sufficient force (about 10 kgf) is applied. -- We observe, moreover, a hysteresis phenomenon --."

Following these hints, we obtained roughly reproducible behavior. Powder column height was kept to 1.0 to 1.2 mm. Significant arm/body pressure, with some electrode piston rotation, was employed. In addition, a calibration scheme with other variously prepared powders was introduced. These included a hydrogen-reduced ferromagnetic metal powder, and a deliberately well-coated magnetic metallic powder. Under these conditions, we obtained the results given in Table 2. On the basis of these results, we conclude that the gas-atomized Ni-Cr powder prepared from the ingot Ni92Cr8 should meet the insulated particle criterion for our artificial dielectric.

8

Table 2

RESISTANCE OF ALLOY POWDER COMPACTS

Sample-Powder	Approx. Resistance
Ni-Cr < 37μm	10^5–10^6 Ω
Reduced Magnetic Metal < 37μm	10^1 Ω
Well-Coated Magnetic Metal $14 < d < 27\mu$m	> 10^7 Ω

II.1.6 Preparation of Artificial Dielectric Composites

II.1.6.1 Selection of Binder for Artificial Dieletrics

The goals of the program call for investigation of artificial dielectrics in two different insulating binders. Our plans have been to use one polymeric binder (for which ϵ' is typically 3 ± 0.5) and one inorganic binder for which ϵ' may be in the range 5 to 10. For the first of these there is an easy choice for a laboratory system, i.e., polyurethane, known commercially as Permuthane™ (Division of Beatrice Foods, Corwin St., Peabody, MA, 01960). It has been used extensively in composites and our collaborators at GE-Aircraft Engine Group, Evendale, Ohio have carried out the preparation of test specimens for us. For the second binder, we asked them to try a proprietary developmental inorganic binder. This has not worked out well, as will be described below. We are currently discussing the possibility of using another moderately high dielectric constant proprietary binder as a substitute.

II.1.6.2 Preparation of Polyurethane Test Speciments

For our initial series of measurements, a set of nine test coupons was prepared. These involved several particle sizes, for reasons which will be explained in a later section. The basic specifications are given in Table 3, including measured values of p determined as described below in Section II.1.6.3.

The preparation followed guidelines for curing the polymer as prescribed by the manufacturer. Suitably chosen amounts of alloy powder and binder powder were combined and blended for several hours. The mixture was leveled into a 2.5 cm x 5 cm (1 inch x 2 inch) die to a thickness such that the final coupon would be ~1 mm (~0.040 in.). The loaded cold die was placed on hot press platens, heated under light pressure from both platens, then with increased pressure, reaching a curing temperature of 177C where it was held for 5 min. It was subsequently cooled under cold running water.

The weighing calculations were based on a cured Permuthane density of 1.06 to 1.11 g/cm³. (For sample ONR 1, we determined 1.11 g/cm³.) These densities, as well as those for the composites are obtained from dimensions on regular shapes and weight. This avoids the possible problems of porous media, etc., but does permit small uncertainties in the determinations. For the alloy, we used a density of 8.79 g/cm³ based on the magnetic determination of composition and an x-ray lattice parameter value of $a_o = 3.529\pm 0.006$A.

II.1.6.3 Evaluation of Volume Loading

As indicated in Section II.1.1 we place emphasis on a straightforward and non-destructive approach to determining the volume loading, p, of metal in the artificial dielectrics, as a guide to analysis of their electromagnetic properties. Our approach to this is through magnetic measurements at low temperature, having chosen an alloy metal that has its Curie point below room temperature.

A few simple formulas are helpful here. The subscripts a, b, c and h will refer to alloy, binder, composite and holes or voids respectively. Although we use the symbol p to designate volume loading in the bulk of this report, for this discussion we shall use the symbol f with the superscript w or v to

9

Table 3

DESCRIPTION OF POLYURETHANE
TEST COUPONS (ALLOY-Ni$_{92}$Cr$_8$)

Sample #	Alloy Particle Size (in μm)	Nominal Alloy Volume Loading, p	Measured Volume Loading, p
ONR 1	—	0	—
ONR 2	+20 - 37	0.40	0.413
ONR 3	+20 - 37	0.30	0.307
ONR 4	+20 - 37	0.20	0.200
ONR 5	+20 - 37	0.10	0.112
ONR 6	+10 - 20	0.40	0.396
ONR 7	−10	0.40	0.384
ONR 8	−10	0.20	0.208

indicate weight fraction or volume fraction. The symbols σ, M and ρ designate magnetization per gram, magnetization per unit volume (e.g., cm^3) and specific gravity (or density in g/cm^3).

For specific magnetization, or magnetization per gram, of composite we write

$$\sigma_c = \sigma_a\, f_a^w + \sigma_b\, f_b^w + \sigma_h\, f_h^w,$$

but obviously $\sigma_h = 0$ and $f_h^w = 0$ at all times, and thus $f_a^w + f_b^w = 1$. Therefore we have $\sigma_c = \sigma_a\, f_a^w + \sigma_b\,(1-f_a^w)$. This expression become trivial but useful when one notes that $\sigma_b = 0$ in most cases of interest. Therefore the formula for weight fraction of alloy becomes $f_a^w = \sigma_c/\sigma_a$. Simply the measurement of σ_c along with a knowledge (or independent measurement) of the alloy magnetization gives its weight fraction.

For volume magnetization and the related volume fractions, we obtain in the same manner

$$M_c = M_a\, f_a^v + M_b\, f_b^v + M_h\, f_h^v,$$

but this time f_h^v may be different from zero although $M_h = 0$ at all times and $M_b = 0$ in most cases of interest. Note also that $f_a^v + f_b^v + f_h^v = 1$, by definition. The formula for volume fraction of alloy, p, is thus

$$p \equiv f_a^v = \frac{M_c}{M_a} = \frac{\rho_c\,\sigma_c}{\rho_a\,\sigma_a} = f_a^w\,\frac{\rho_c}{\rho_a}.$$

This requires the additional measurement (or knowledge) of the density of the composite and of the alloy. With these measured values, on whole samples, the results are on firm ground and contain no approximations or idealizations. We discuss determination of the void fraction in a later section.

As for the case of the binder alone, we have obtained more consistent results in determining density in the "primitive" way from dimensions on regular shapes and weight. For many electromagnetic considerations it is the overall volume property which is of interest, so that this simple method which includes voids, cracks, etc., is the proper one. The results for the volume loading determinations are given in Table 3. The agreement between nominal and measured values is very satisfactory and should be characteristic of polymeric-type binders when appropriate care is taken. With other categories of binders such agreement cannot be taken for granted.

II.1.6.4 Preparation of Inorganic Binder Composites

For a second binder choice for the composite artificial dielectrics, we tried to use a proprietary inorganic binder currently under development at GE-Evendale. It is intended for a similarly-sized but chemically different dispersoid (loading material). Typically, with inorganic binders there is a high temperature cycle to bring the binder to its final state. In our past experience [1] such a high temperature excursion may be accompanied by chemical reaction between binder and dispersoid particle. In the present case we requested 4 composites, p = 0.1, 0.2, 0.3 and 0.4, each with the largest particle size $+20-37\mu$m of the Ni_{92} Cr_8 powder. In each case, the resulting composite was ferromagnetic at room temperature. Indeed a thermomagnetic scan showed Curie points up to 350C (pure Ni, $T_c = 358C$) with strong suggestions of composition variations within the magnetic phase.

Under these conditions it is very difficult to know the alloy composition in the composite. Therefore we could not determine volume loading without destruction and visual or probe analysis of the composite.

Still another proprietary binder with moderately higher ϵ' is being developed at GE-Evendale. ($\epsilon' \cong$ 5). In the coming period we hope to be able to make composites with this binder which is less demanding of the dispersoid.

Therefore, the sought-for comparison with different permittivity binders has been delayed. We do have a few data points from other concurrent work with this binder which support the expected trend.

II.2 Magnetic Dipole and Particle Size Effects

At first consideration it might seem that purely electric dipole phenomena would fully describe the high frequency response of an artificial dielectric composed of strictly non-magnetic materials (in contrast to prior work on artificial magneto-dielectrics [1]). Indeed this appears to have been the initial point of departure for analysis over the past rather active decade of research on selective absorbers of solar and infrared radiation [17,18]. However, it was quickly realized that, if the diameter of the conducting particle is not negligible compared to the skin depth, there is a second, rather classical, mechanism for absorption arising from the effects of the magnetic field of the incident radiation. In the time-varying magnetic field, there will be an induced eddy current magnetic polarization and an eddy current loss. The effective permeability of the composite artificial dielectric will thus not be unity even though the d.c. permeability of the constituents may be exactly unity. These magnetic effects are size-dependent while the electric dipole polarization and loss phenomena are not. Indeed the magnetic contribution dominates for metallic particles above about 50A in size [17,19]!

While this feature was not spelled out in our initial plans for this research program, calculations presented below show that much interesting behavior occurs in relevant frequency and particle size ranges. Therefore, we have put emphasis on obtaining and measuring different powder size fractions. This is the expansion of scope referred to in Section I above, which we have requested to be balanced by suppression of Task 4 of the original program schedule (Table 1). The change has also caused us to subcontract out a small effort at sizing some of the alloy powder by air-classification. Sieving is a sensible mode only for small quantities. This subcontract was not envisaged when the original program plans were submitted.

II.2.1 Magnetic Polarizability of a Single Particle

The magnetic response of an isolated isotropic conducting sphere has been discussed nicely by Landau and Lifshitz [20]. Following their notation,

$$M = \alpha H$$

where M is the magnetization (magnetic moment per unit volume), H is the external magnetic field and α is the (complex) magnetic polarizability. For a sphere they derive (with $\alpha = \alpha' + i \alpha''$),

$$\alpha' = - \frac{3}{8\pi} \left[1 - \frac{3 \delta \left[\sinh (2a/\delta) - \sin (2a/\delta) \right]}{2 a \left[\cosh (2a/\delta) - \cos (2a/\delta) \right]} \right]$$

and

$$\alpha'' = -\frac{9\,\delta^2}{16\,\pi a^2}\left[1 - \frac{a}{\delta}\,\frac{\sinh\,(2a/\delta) + \sin\,(2a/\delta)}{\cosh\,(2a/\delta) - \cos\,(2a/\delta)}\right]$$

where δ is the skin depth given by

$$\delta = \frac{c}{\sqrt{2\,\pi\,\sigma_{EL}\,\omega}} \text{ in cm (with cgs units)}$$

or

$$\delta = \frac{1}{\sqrt{\pi\,f\,\mu_o\,\sigma_{EL}}} \text{ in m (for practical or SI units)}$$

In these expressions $\sigma_{EL} = \dfrac{1}{\rho_{EL}}$ is the electrical conductivity (in appropriate units), f the frequency and μ_o the permeability of free space $(4\,\pi\,\times\,10^{-7}$ henry/m).

In Figure 6 we plot $-\alpha'$, the (negative) real part of the conducting sphere magnetic polarizability as a function of a/δ, the radius divided by the skin depth. In the low frequency (or small particle size) limit, $\delta >> a$, this component decreases as $(a/\delta)^4$. At the other extreme, it reaches a finite value, $\alpha' = -3/8\pi$, corresponding to the magnetic behavior of a superconducting sphere [20].
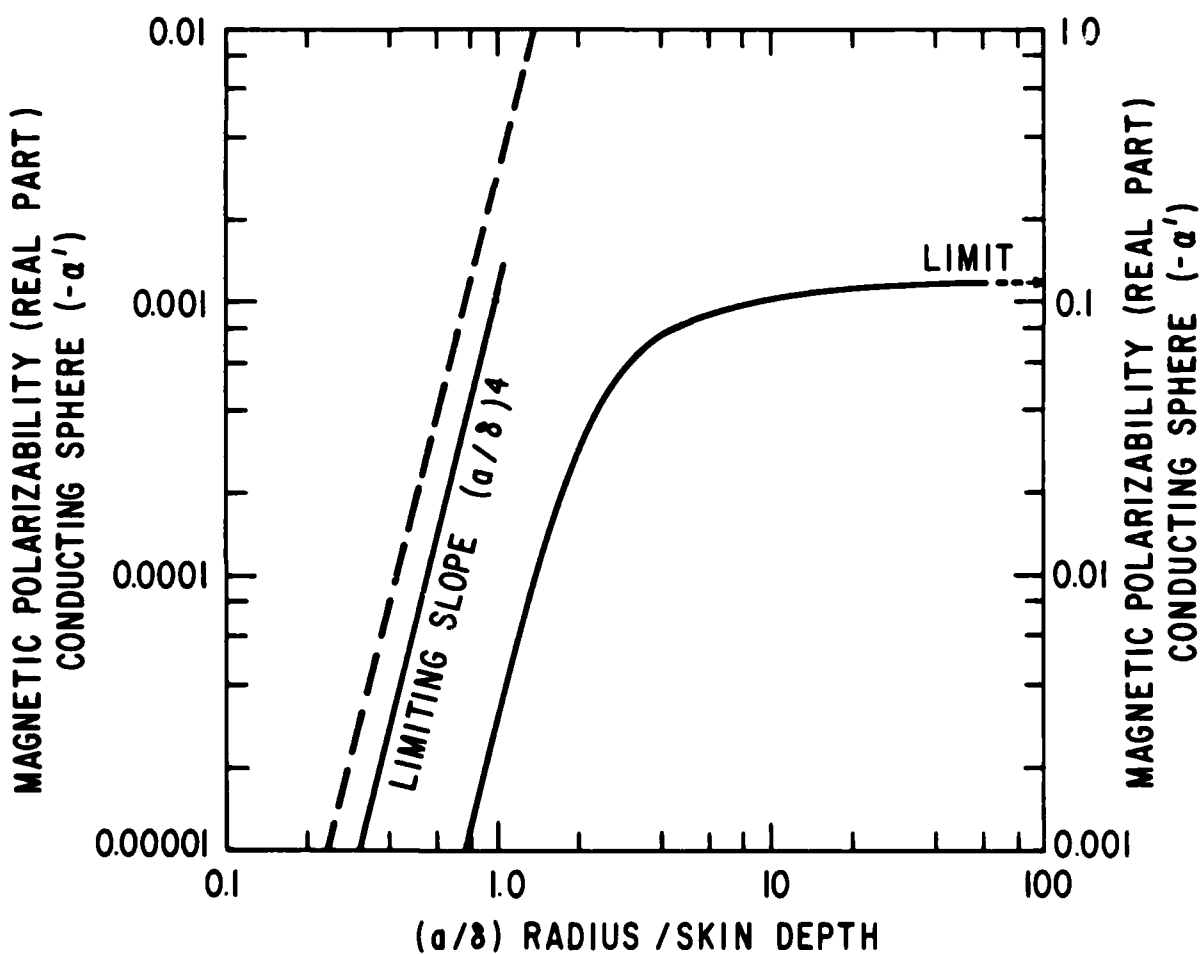

Figure 6. Magnetic polarizability of a conducting sphere. Negative real part, $-\alpha'$, vs. the dimensionless ratio of sphere radius to skin depth.

In Figure 7, the imaginary part of the magnetic polarizability is presented, again as a function of a/δ. This quantity is intrinsically positive. It vanishes in both of the extremes of small or large radius (or frequency); in the former the limiting behavior is as $(a/\delta)^2$, while in the latter it decreases in proportion to δ/a. The maximum loss occurs at $a/\delta = 2.3$, while remaining above half its maximum for the (a/δ) range of 1.2 to 7.

II.2.2 From Single Conducting Sphere to Composite

The magnetic polarizability formulas given in the preceding section pertain only to the spherical shape and the externally applied magnetic field. In describing magnetic properties in general, as well as in the present case of a dispersion of small magnetic particles, one must proceed carefully in accounting for the various demagnetizing effects, internal and external fields, etc. For example, in the present case one may have to distinguish between the demagnetizing coefficients of the overall composite sample, of the individual particle, and of the cavity "constructed" around the particle in analyzing for interactions between the particle's dipole moment and the magnetization of the particles. In our model, the latter interactions are considered in the mean-field approximation which is accurate in the dilute limit. (We shall describe some of its weaknesses in a later section when we deal with the dielectric behavior). As another example, particularly relevant to conventional magnetic materials, i.e., ferromagnetic ones, the quantity of fundamental importance is the intrinsic or internal property, be it susceptibility, permeability or polarizability.

For the artificial dielectric composites studied here, we have the simple case of spherical particles (demagnetizing coefficient = $4\pi/3$), spherical cavity (same) and overall sample configurations for which we can ignore demagnetization. The latter come about because the measurements are carried out with closed flux configurations (toroid in a co-axial line) or thin slabs with the incident H-field parallel to the slab plane.
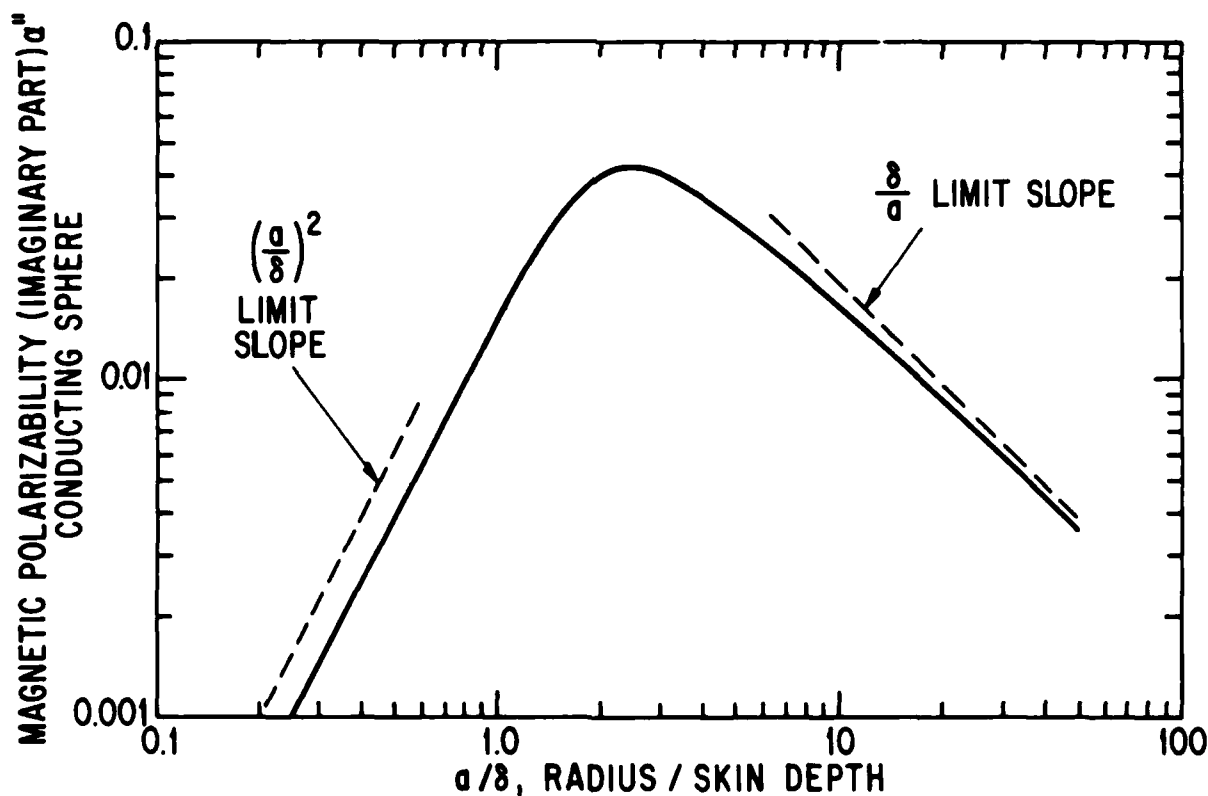

Figure 7. Magnetic polarizability (imaginary or loss part) of conducting sphere in time-varying field. α'' vs. (a/δ).

Having hoisted the flags of caution, we shall not repeat the derivations which may be found in appropriate textbooks, but shall merely present some key formulas. The intrinsic (or internal) magnetic susceptibility of the sphere (relative to the internal field) is related to the polarizability derived above as:

$$\chi_i = \frac{\alpha}{1 - 4\pi\,\alpha/3}$$

For a composite of spherical particles with volume loading, p, the susceptibility relative to an externally applied field is:

$$\chi_{ext} = \frac{\chi_i p}{1 + \frac{4\pi}{3}\chi_i - p\,(\frac{4\pi}{3} - N_s)\,\chi_i},$$

where N_s is the demagnetizing coefficient for the overall composite sample shape. In the common case herein, we have $N_s = 0$, and thus we obtain

$$\chi_{ext} = \frac{p\,\chi_i}{1 + \frac{4\pi}{3}(1-p)\,\chi_i}.$$

Upon substituting the relation between χ_i and α, this formula becomes

$$\chi_{ext} = \frac{p\,\alpha}{1 - \frac{4\pi}{3}\,p\alpha}.$$

This appears so simple that one presumes it could have been found more directly. However, we feel the excursion into details and warnings is appropriate. Finally for the permeability, we have, by definition, $\mu_{ext} = 1 + 4\pi\,\chi_{ext}$ and then

$$\mu_{ext} = \frac{1 + 2\,(\frac{4\pi}{3})\,p\,\alpha}{1 - \frac{4\pi}{3}\,p\,\alpha}.$$

At this point we take note that α and hence μ are complex, with the forms $\alpha = \alpha' + i\,\alpha,$" $\mu = \mu' + \mu.$" Making these substitutions and continuing the manipulation, we obtain

$$\mu_{ext}' = \frac{1}{D}\left\{1 + \frac{4\pi}{3}\,p\,\alpha' - 2(\frac{4\pi}{3}\,p)^2\,[(\alpha')^2 + (\alpha'')^2]\right\},$$

$$\mu_{ext}'' = \frac{4\pi\,p\,\alpha''}{D}$$

with

$$D = 1 - 2(\frac{4\pi}{3})\,p\,\alpha' + (\frac{4\pi}{3}p)^2\,[(\alpha')^2 + (\alpha'')^2].$$

In Figures 8 and 9 we show the behavior of μ_{ext}' and μ_{ext}' for values of p from 0.1 to 0.5. As will be discussed later, the empirical limit for random packing of monodisperse spheres is about 0.63, but in practice one rarely goes much beyond about 0 5. In Figure 8, we note that the negative real polarizability manifests itself in a substantial lowering (diamagnetic tendency) of μ' from unity. In Figure 9, the family of curves for μ'' are straightforward reflections of the behavior of α'' (as given in the formula). These formulas and graphs are in a universal dimensionless form, expressed in terms of a/δ. It remains to demonstrate that the changing properties are relevant to the materials and electromagnetic parameters of this investigation.

II.2.3 From Model Composite to Practical Application

At this point we transform the model calculations, expressed in dimensionless ratios of material parameters, into real units that are measurable. The major parameter is the resistivity, followed by particle sizes and frequencies of interest. The resistivity, ρ_{EL}, for the alloy $Ni_{92}\,Cr_8$ is $55 \times 10^{-8}\,\Omega$ m [21].
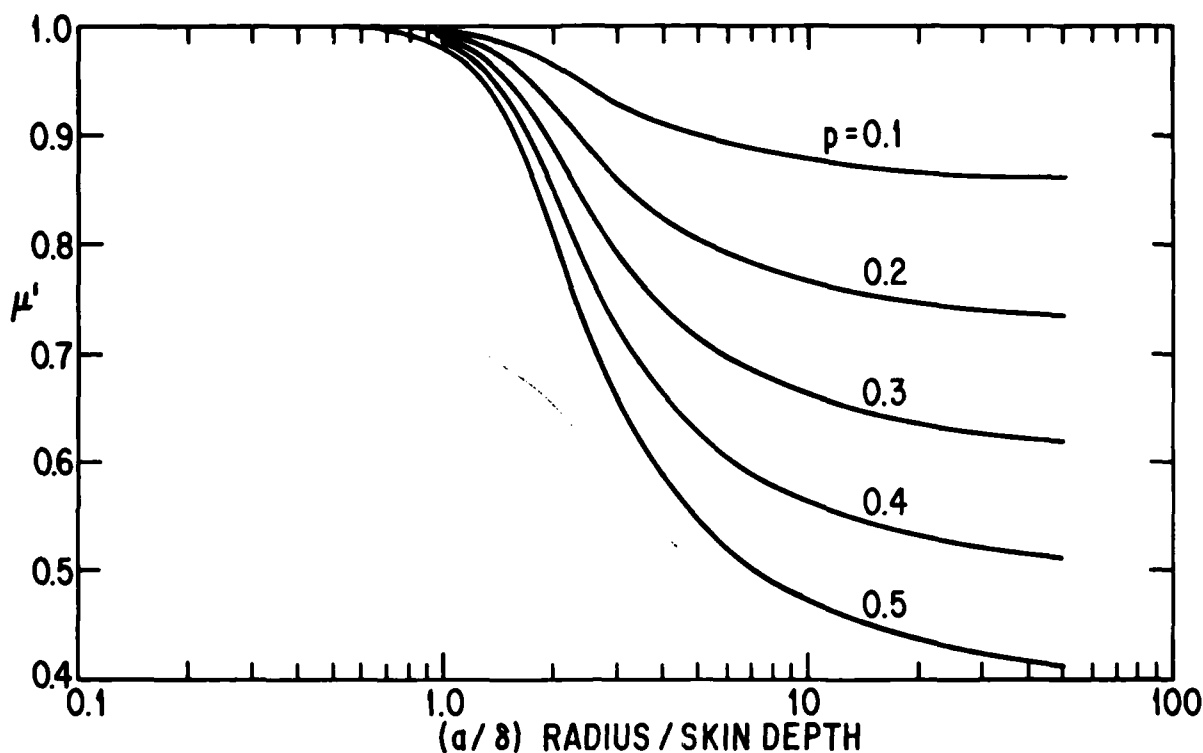
Figure 8. Magnetic permeability (real part) calculated for composites of conducting spheres at various volume loadings, p; μ'_{ext} vs. (a/δ).

When this is substituted into the formula for skin depth, δ, we obtain at 10GHz, δ = 3.7μm. Proceeding a step further with the consideration that peak α'' (and μ'') occurs at a/δ = 2.3, we find that "important" sphere *diameters*, d_c are as follows:

$$d_c = 17\ \mu m\ at\ 10GHz$$
$$d_c = 7.6\mu m\ at\ 50\ GHz$$
$$d_c = 5.4\mu\ at\ 100\ GHz$$

Obviously there is relevance for a powder with particles below 37μm (-400 mesh).

We show in Figures 10 and 11, the calculated model behavior for μ' and μ'' for this alloy composition, for a volume loading, p = 0.4, and for various sphere diameters of interest, i.e., 5, 10, 20 and 30μm (Similar calculations for other p-values are presented below). It should be noted that our calculations above have been in the c.g.s. system for which μ', μ'' are dimensionless. As we move closer to real electrical measurements in the "more practical" m.k.s. SI system, these expressions or graphs of $\mu'\ \mu''$ (and later of ϵ',ϵ'') are to be considered as *relative* to the permeability (or permittivity) of free space. In other words we have $\mu_r' = \mu'/\mu_o$, etc.

The qualitative remarks made for Figures 8 and 9 remain true for these figures. However, the separation of the features for the various sphere diameters is rather dramatic. It certainly invites experimental demonstration in that the range of sizes and of frequencies for this investigation spans the calculated behavior very nicely. It is for these reasons that we prepared samples with different particle sizes (and volume loadings) as listed in Table 3; i.e., −10μm, + 10−20μm, and + 20−37μm.

It is instructive to extend the critical diameter/frequency consideration somewhat further on either end. If we move to the far-infrared, to a frequency of 1 THz (1 x 10¹²Hz) alternatively expressed in wave numbers as 33cm⁻¹, the critical diameter for maximum absorption in this alloy would be 1.7μm

15
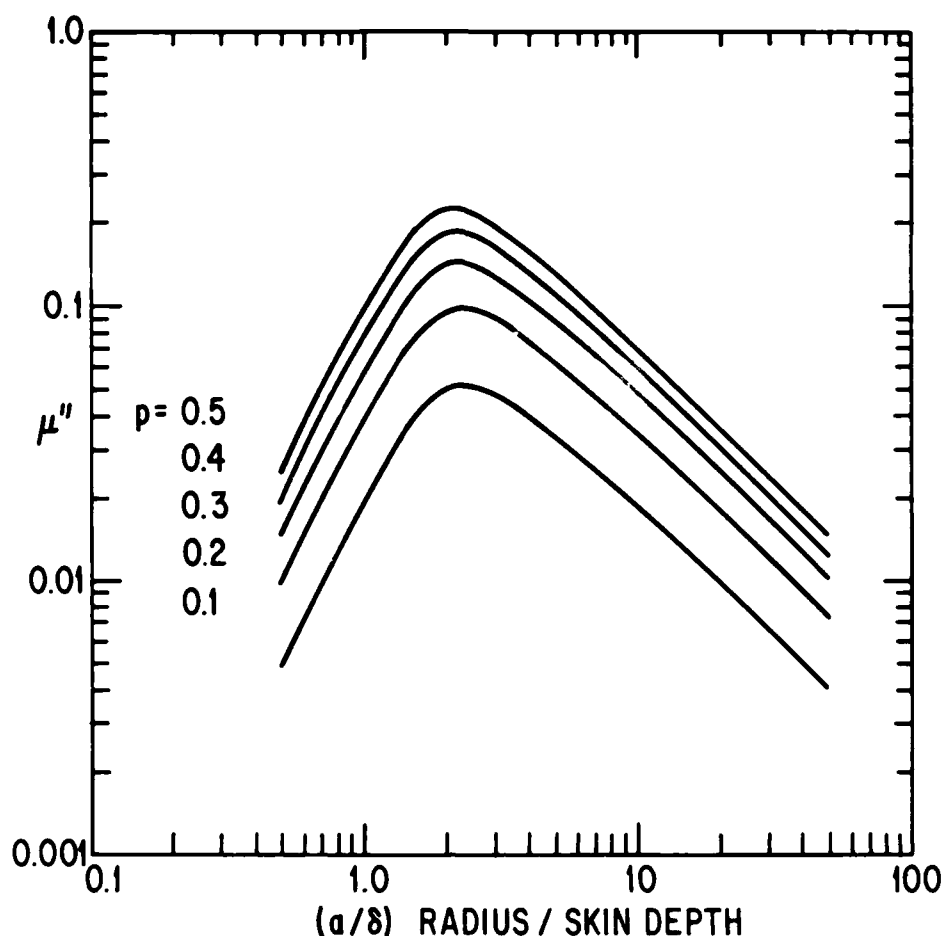
Figure 9. Magnetic permeability (imaginary part) calculated for composites of conducting spheres; μ''_{ext} vs. (a/δ) for various volume loadings, p.

which is in line with predictions for such research [19]. This domain is of interest for selective absorbers of solar or i.r. radiation. At the other extreme, that of low frequency, the critical diameter at 10 kHz is 1.7 cm. This is in the regime for induction heating!

In each of these two limiting regions one is unlikely to find results obtained and presented in terms of the complex permeability (and permittivity). Instead the focus is on absorption per se, because of measurement techniques as well as because of practical interest. For these reasons, measurements of the permeability reported here make a useful contribution to the understanding of artificial dielectric materials in the microwave frequency region and they relate to the nearby far-infrared region also. At present, we are aware of only one report which presents these kinds of measurements and analysis. It deals with systems of millimeter-sized ferromagnetic steel spheres over the kilohertz and megahertz frequency range [22].

There is yet another interest in such model results, a technological one. The RAM physics model [1] predicts that high frequency loss in a magneto-dielectric should become negligible beyond certain frequencies and/or temperatures (depending on material parameters). When the induced magnetic effects are included, one may expect to find lossy properties outside the limits indicated previously. An example of this is presented in the classified Appendix.
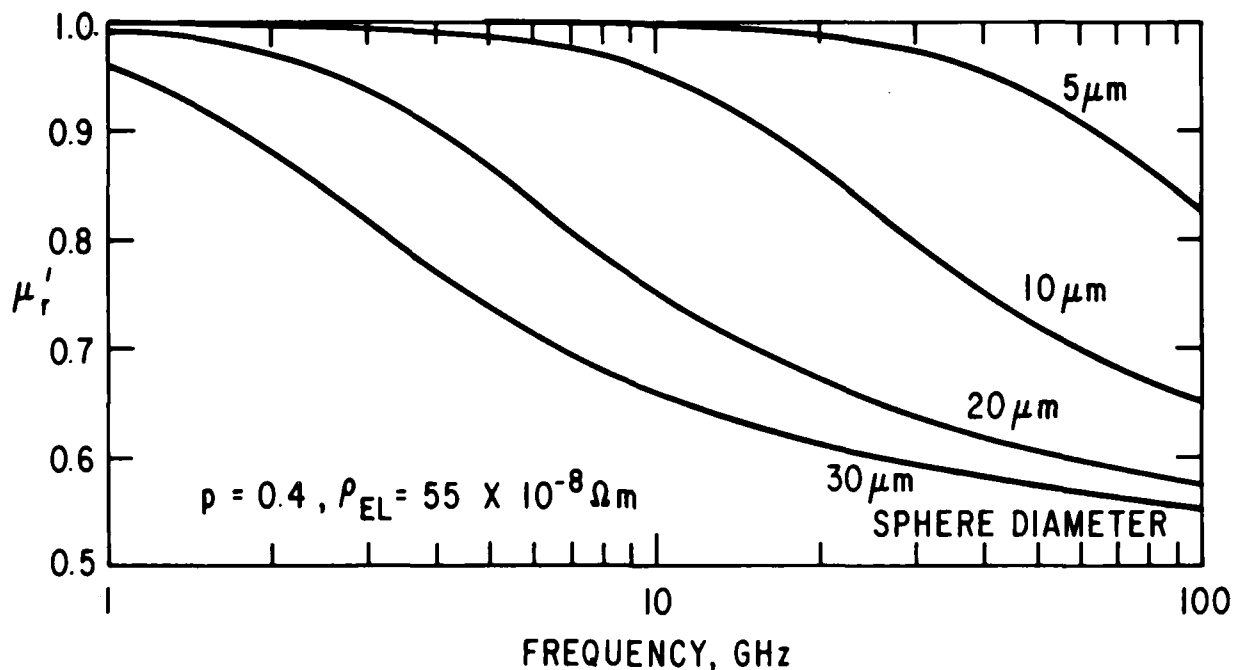
16

Figure 10.   Relative real magnetic permeability, μ_r', vs. frequency calculated for composites
of conducting spheres of various diameters; composite volume loading, p = 0.4;
sphere alloy resistivity, ρ_{EL} = 55 x 10^{-8} Ω m.

II.2.4 Measurement of High Frequency Magnetic Permeability and Permittivity

Measurements of the constitutive parameters, complex μ_r and complex ϵ_r, are being made in the centimeter wavelength range, ~3-18 GHz, at GE-CRD. The equipment is based on a Hewlett-Packard Network Analyzer. The major building blocks of the system are the 8620A Sweep Generator, the 8410A Network Analyzer, the 8411A Harmonic Frequency Converter, the 8412A Phase-Magnitude Display, the 8746B S-Parameter Test Set, and the 905A Coaxial Sliding Load for calibration runs.

Analog-to-digital converters, together with a data logger and a T.I. Terminal make it possible for the Network Analyzer to interface with a CRD main frame computer. Any given frequency band of the 8620A Sweep Generator may be swept with a step size of 0.1, 0.2, 0.5, 1, 2, or 5%. Steps of 1% have been chosen for this characterization work. This enables many data points to be taken so that spurious points are of no significance and confidence can be generated that just cannot be obtained when widely separated spot frequency measurements are taken. This "overview" approach is facilitated by a screen display of the calculated μ and ϵ values from which display a hard copy can be obtained. Smoothing by visual inspection and/or a drawing curve or straight edge completes the process. Alternatively, a tabulation of the measured values can be obtained.

Several methods of measuring the complex permeability and permittivity are suitable for use with a network analyzer. Of these, the reflection technique (S_{11} scattering coefficient) employing first a single-thickness, then a double-thickness sample placed in front of an RF short is the technique used here.

Since the S-parameter terminals of the network analyzer have precision APC-7-type coaxial connectors, the sample holder was made to interface as smoothly as possible with this type connector. The precision outer (0.2756-inch, 7mm) and inner (0.1197-inch) conductors are available commercially and were used to construct the coaxial line sample holder. The dimensions of a toroidal sample are 0.275 inch O.D., 0.120 inch I.D., and about 0.040 inch thick. (The sample thicknesses of the pair used for a particular set must be identical). An attempt is made to permit no more than 0.001 inch clearance

17
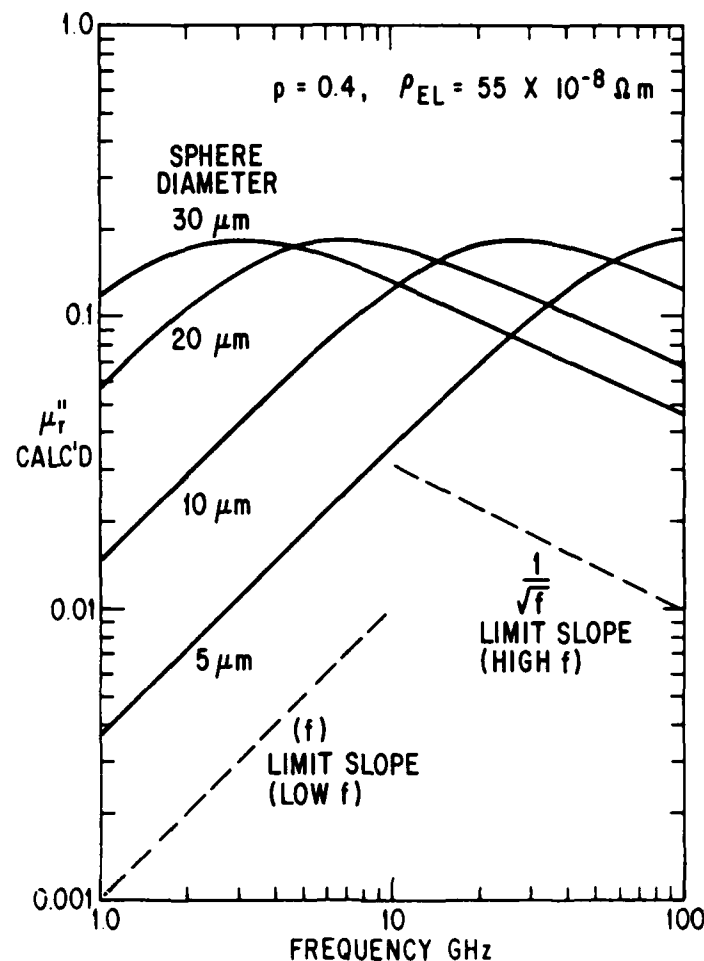
Figure 11. Relative imaginary magnetic permeability, μ_r'', vs. frequency calculated for composites described in Figure 10.

between the sample and its holder. In Figures 12-17 we show examples of these measurements for μ_r',μ_r'' in the 6-12 GHz band for samples ONR #2, #4, #8. The first two are for powder with diameters in the range 20μm to 37μm, loadings $p = 0.4$ and 0.2 respectively. The third of these samples is for powder with $d < 10\mu$m and $p = 0.2$. (cf. Table 3). The figures show the plotted data and the smooth curve used for subsequent evaluation.

We are currently working to extend these results within the centimeter range. In addition we have requested our colleagues at GE-Re-Entry Systems Operation, Philadelphia, to carry out measurements at 35GHz. Initially it was planned in the Contract Proposal that all measurements above the 12 GHz or 18 GHz range (specifically at 35 and 94 GHz) would be carried out at the Naval Research Laboratory. However, we were somewhat dismayed by their requirement of a 5 in. x 5 in. seamless square sample for the 35 GHz measurement in the arch method. By contrast, the equipment at GE-RSO uses a single 1/4 in. diameter disc in a circular waveguide cavity. The measurements are in progress at the time of this writing. (This is another unanticipated reason for a subcontract which was not scheduled at the start of the program).

Figure 12.   Relative real permeability measurements, μ_r' vs. frequency; range 6-12 GHz.
Sample ONR #2, p = 0.413, sphere diameter $20 < d < 37\mu$m. Data curve for
100 points and smoothed line.

Figure 13.   Relative imaginary permeability measurements, μ_r'' vs. f; same sample and fre-
quency range as in Figure 12.

Figure 14. Relative real permeability measurements, μ_r' vs. frequency; Range 6-12 GHz, Sample ONR #4, p = 0.200, sphere diameter $20 < d < 37 \mu$m. Data and smoothed curve.

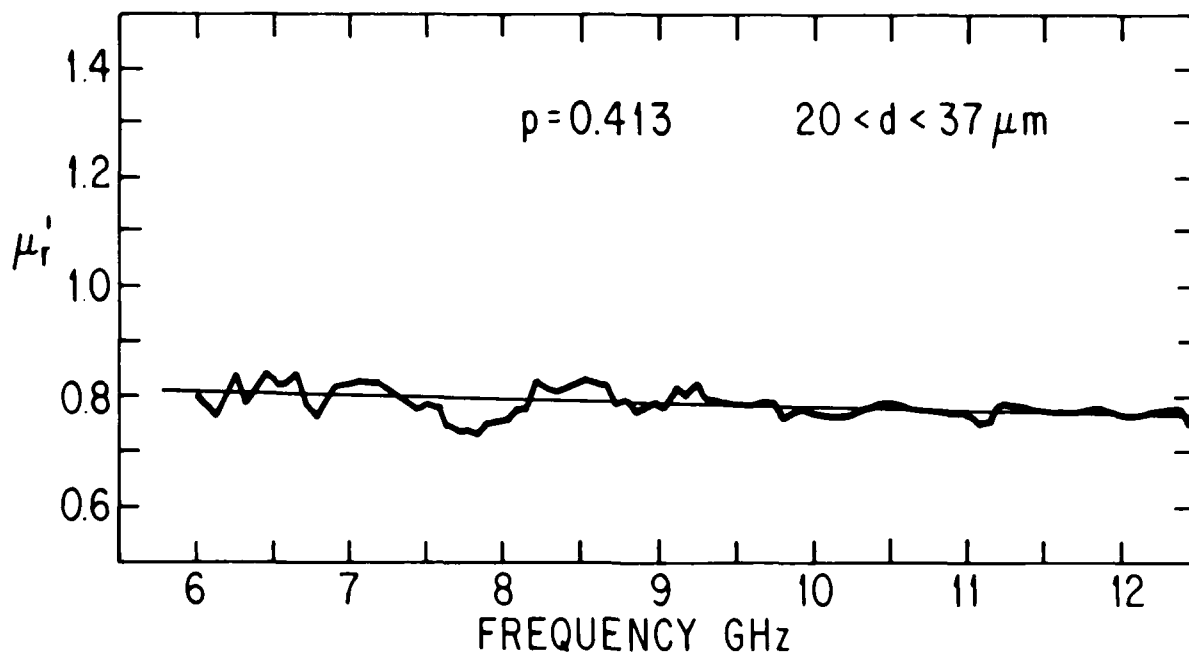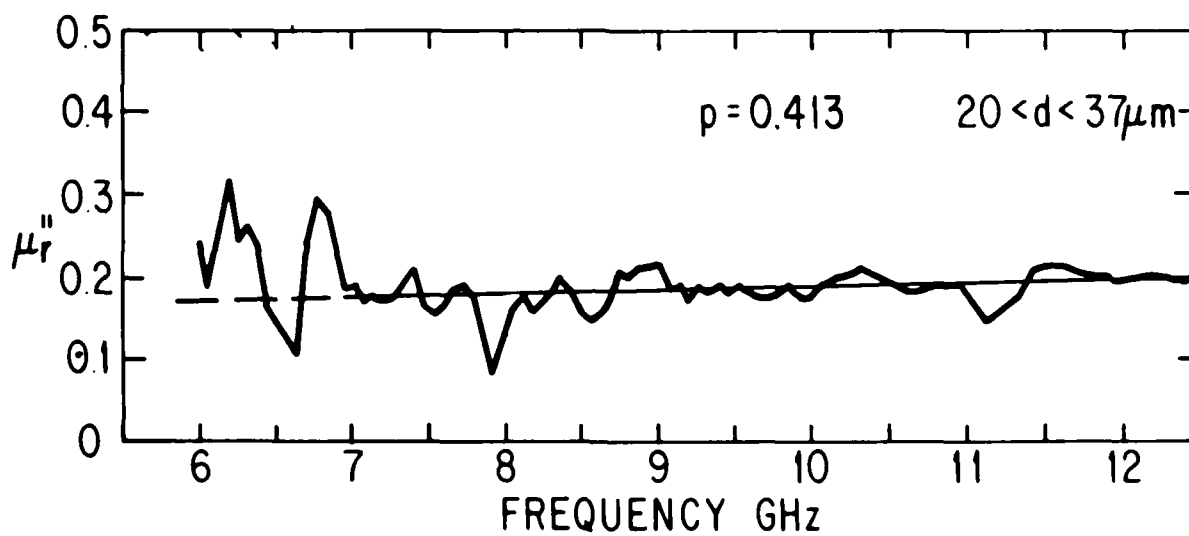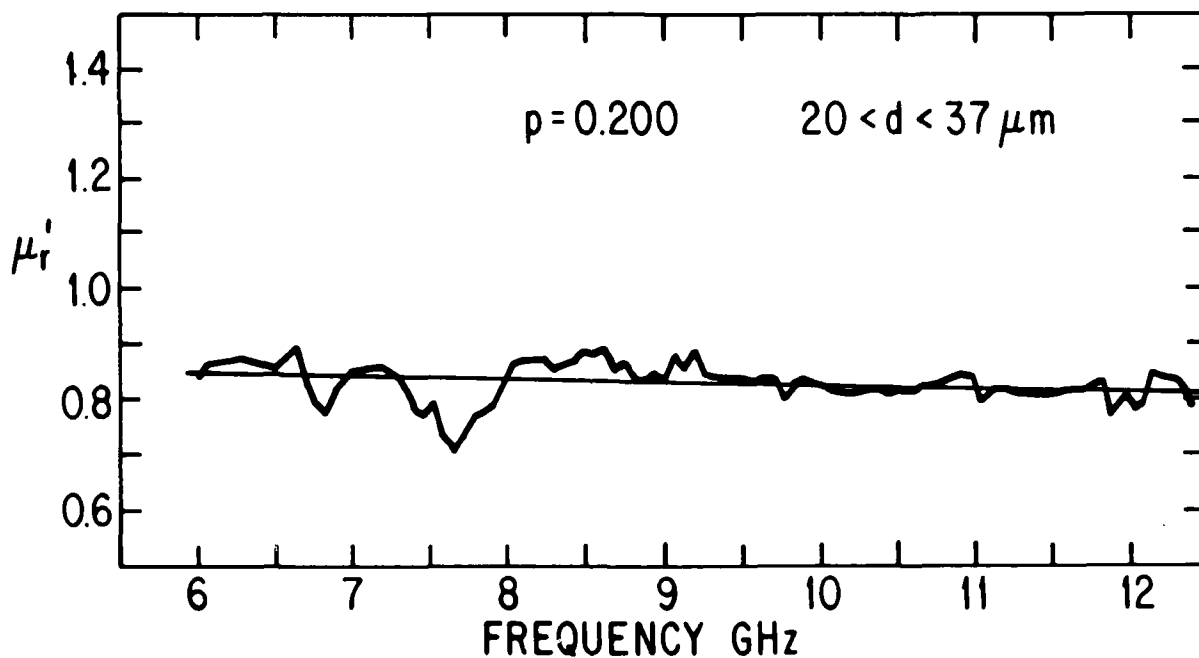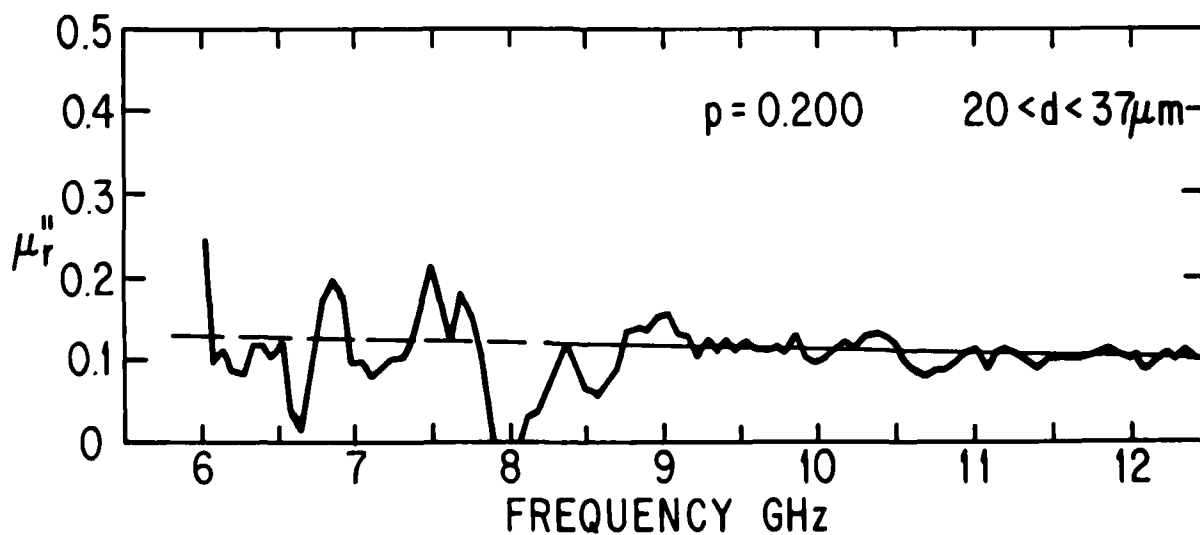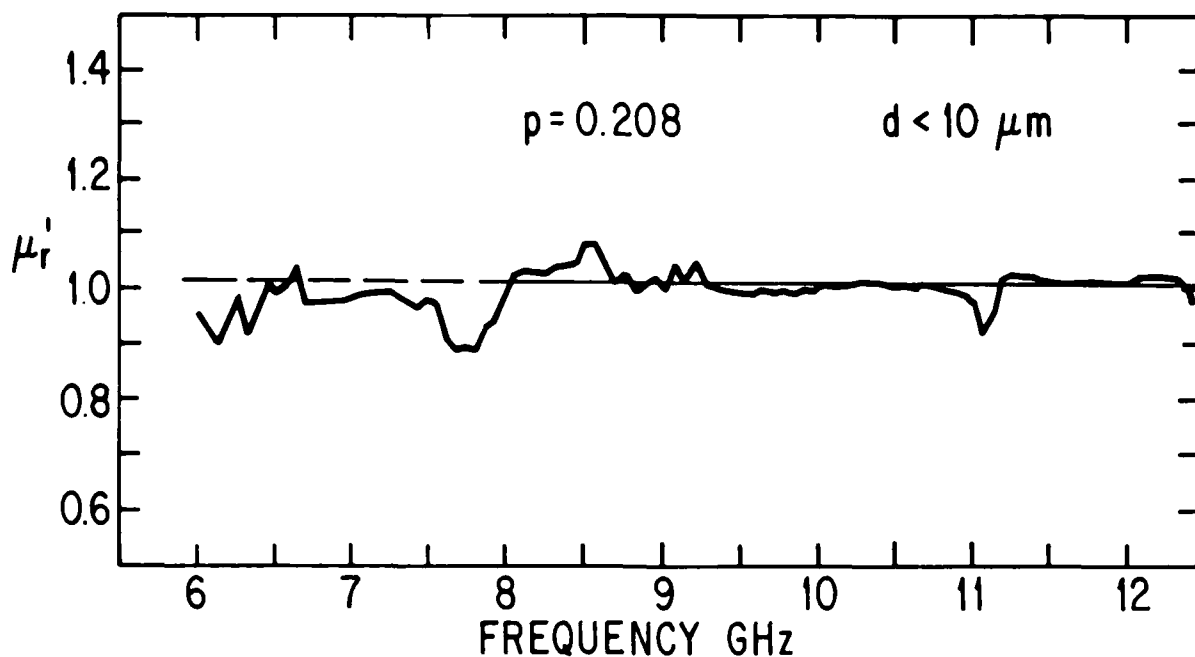**Figure 15.** Relative imaginary permeability measurements, μ_r'' vs. f; same range and sample as in Figure 14.

20

Figure 16.   Relative real permeability measurements, μ_r' vs. frequency; Range 6-12 GHz, Sample ONR #8, p = 0.208, sphere diameter d < 10μm.
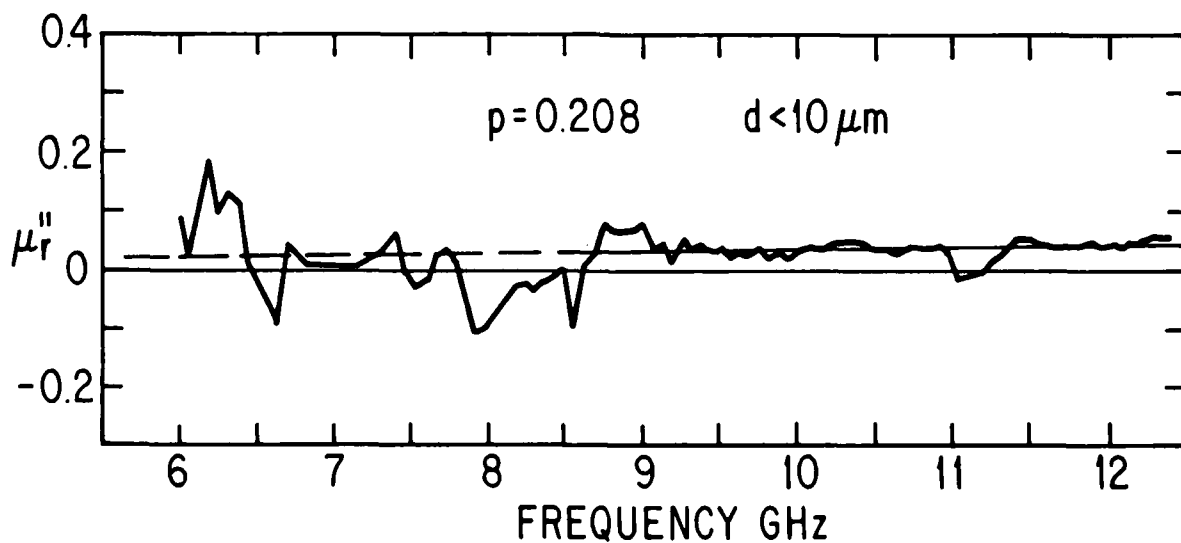
Figure 17.   Relative imaginary permeability measurements, μ_r'' vs. f; same range and sample as in Figure 16.

II.2.4.1 Comparison of Permeability with Model Calculations

From measurement curves of the type just presented we can read the smoothed curve values at a few (say 2 or 3) frequencies. A Gerber Variable Scale, Model TP007100B, is rather useful at this stage. These readings can be transposed onto graphs of the type shown in Figures 10, 11, i.e., the model calculations for μ_r', μ_r'' vs. frequency for various volume loadings and various particle diameters.

These calculations with the data for the seven samples measured in the range from 6 to 12 GHz are shown in Figure 18-25. These go in pairs, first μ_r' then μ_r'', each for the four p values (0.4 down to 0.1). In two of the four p-value cases we have 2 or 3 particle size ranges. The agreement between measured data and calculated values is qualitatively quite good and even quantitatively rather acceptable in most examples. The experimental demonstration of the predicted and obviously non-trivial-in-magnitude behavior is an important step in the accommodation of artificial dielectric materials to millimeter wavelength applications.

As we extend these measurements to higher (and lower) frequencies, the quality of the demonstration will become more dramatic. At this point, the importance of this diversion in the research program has been clearly established.

II.3 Microstructure of Artificial Dielectric Composites: Observations and Implications

A significant task envisioned in the planning of this investigation, as shown in Table 1, and amplified in the Proposal Work Statement is to "Analyze the effects of microstructure control, e.g. porosity, passivation coating, packing, on the dielectric behavior of oxide-passivated metal-insulator composites." This task was motivated by a basic question posed in Section I, i.e., the relationships between previously observed dielectric behavior and the simple Maxwell model, its range of validity out to higher [1] volume loadings than sustained by many other composites, and the observed deviations from the simple model behavior.
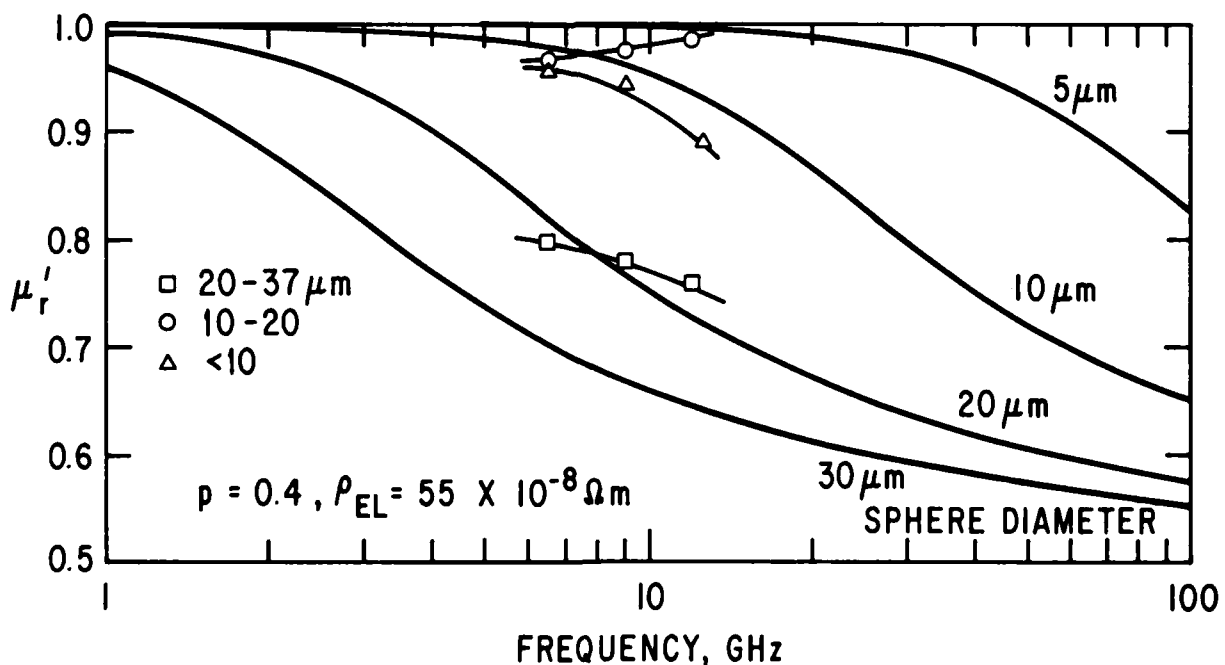
Figure 18. Comparison of Experiment and Model Calculations, μ_r' vs. f, p = 0.4.
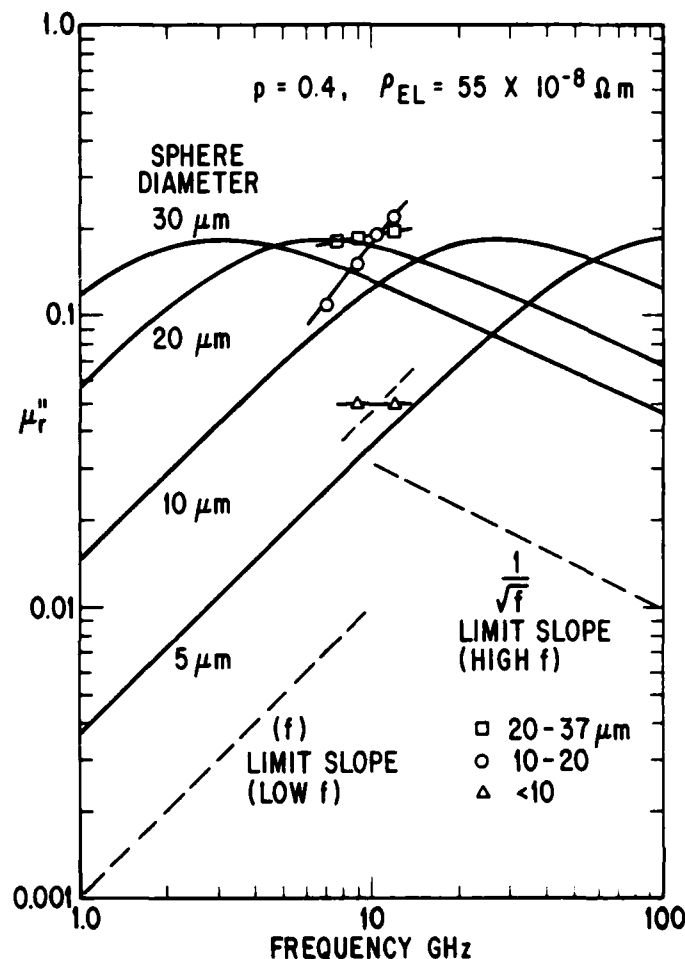
Figure 19. Comparison of Experiment and Model Calculations, μ_r'' vs. f; p = 0.4.

We cannot complete a discussion of these questions and factors at this point, in part because the investigation is still in progress both experimentally and analytically, and in part because it depends on a more thorough exposition of theoretical treatments of composite dielectrics which comes later in this report. While this is a bit of a chicken and egg problem, we can make a start on the observations which are, or may be, possible and introduce their relevance in at least a sketchy way.

II.3.1 The Insulating Coating

In Section II.1.5 we reported on the surface condition of the metal powder prepared by gas-atomization. From magnetic Curie temperature evidence, from Auger electron spectroscopy and from powder resistivity measurements we concluded that the atomized powder particles have an insulating coating. In several rough approximations we estimated the oxide coating thickness at about 0.1 to 0.2μm.

It would be rash to call this a passivating layer, however. This conclusion derives from the considerable reaction suffered by this alloy powder when composite preparation using an inorganic binder was attempted. That reaction was evidenced in the thermo-magnetic scan.

The presence of the insulating coating is very significant for the electromagnetic behavior, especially for the dielectric properties. Loosely speaking, it prevents the individual metal particles from shorting
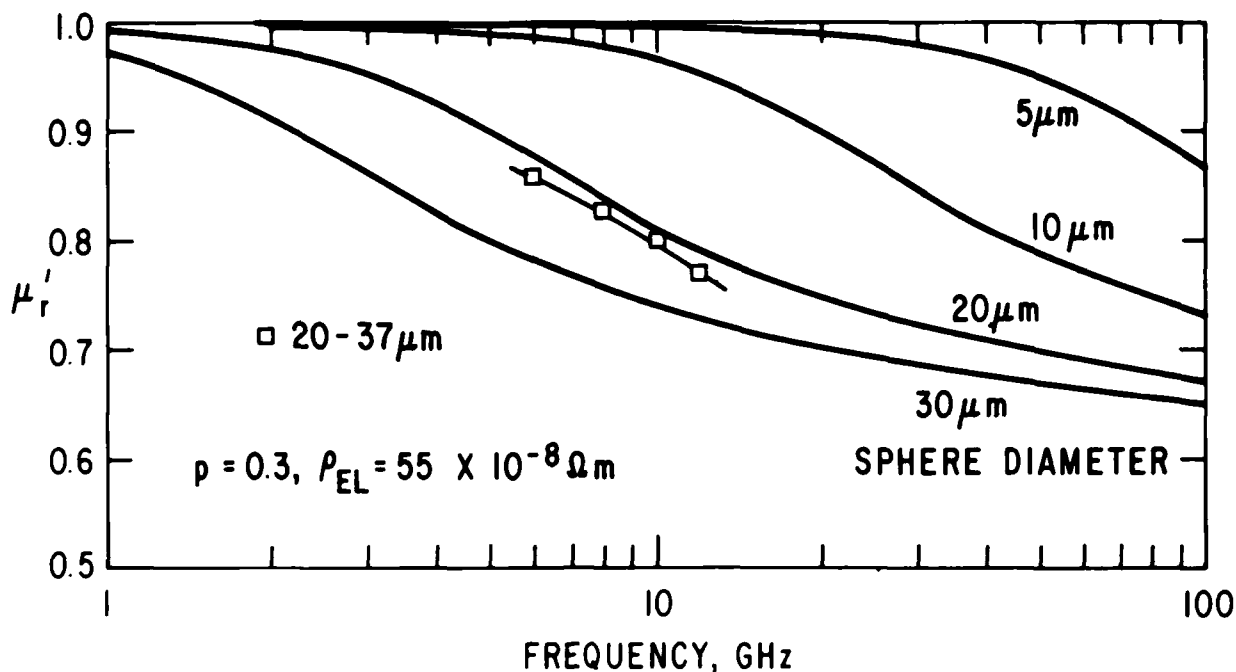
Figure 20. Comparison of Experiment and Model Calculations, μ_r' vs. f; p = 0.3.

to each other. More elegantly, it means we have a correlated heterogeneous medium in which conducting particles are completely surrounded by insulating material. This restricts the theoretical approach to describing the dielectric behavior in a favorable way. Volume loadings up to or approaching the packing limits can be achieved with coated particles (spheres) without the establishment of conducting paths, i.e., percolation.

With a coating on the conducting sphere, as well as a binder material, the resulting composite is a three-phase medium. However, it is possible to replace the coated sphere combination by a single, slightly modified, dielectric sphere. We shall return to this in a later section, but it suffices to say that, for the very thin coatings estimated herein, the coated metal sphere dielectric constant is sufficiently high compared to that of the binder that the properties of the resultant composite ϵ' are unchanged.

II.3.2 Calculation of Porosity

An aspect of the microstructure of composites is the porosity, i.e., the volume fraction of holes or voids. It is straightforward to calculate this quantity using the densities of the separate components and their proportions ascertained from observable measurements. We refer back to definitions of symbols used in Section II.1.6.3 for evaluation of volume loading.

Consider a mass m_c of the composite occupying volume v_c. Then

$$v_c \, \rho_c = m_c = v_c \, (\rho_a \, f_a^v + \rho_b \, f_b^v + \rho_h \, f_h^v),$$

but, $\rho_h \equiv 0$, of course. Thus we have

$$\rho_c = \rho_a \, f_a^v + \rho_b \, f_b^v, \text{ or}$$

$$f_b^v = \frac{\rho_c - \rho_a \, f_a^v}{\rho_b}$$

But with $f_h^v = 1 - f_a^v - f_b^v$, we can write

24

$$p = 0.3, \ \rho_{EL} = 55 \times 10^{-8} \ \Omega m$$

SPHERE DIAMETER

30 μm

20 μm

10 μm

5 μm

□ 20 - 37μm

μ_r''

FREQUENCY GHz
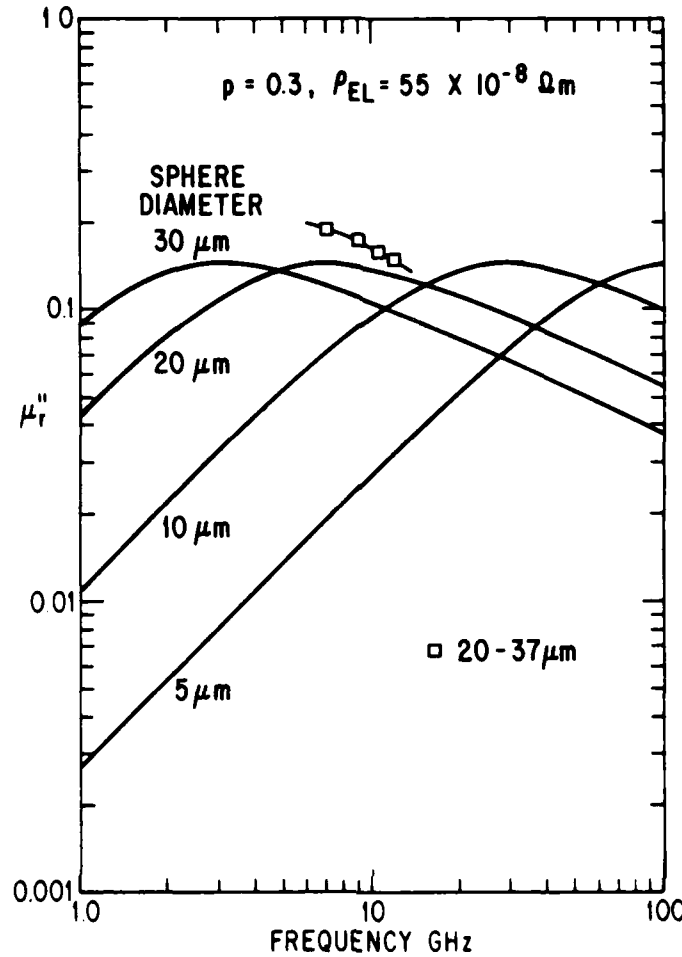
Figure 21. Comparison of Experiment and Model Calculations, μ_r'' vs. f; p = 0.3.

$$f_h^v = 1 - f_a^v - \frac{\rho_c}{\rho_b} + \frac{\rho_a}{\rho_b} \quad f_a^v = 1 - \frac{\rho_c}{\rho_b} + p \ (\frac{\rho_a}{\rho_b} - 1).$$

Alternatively, using the formula for p in observables, we obtain

$$f_h^v = 1 - \frac{\rho_c}{\rho_b} + \frac{\sigma_c \rho_c}{\sigma_a} \ (\frac{1}{\rho_b} - \frac{1}{\rho_a}).$$

The principal sources of error in this determination of porosity are the density values for the binder material and for the composite. By contrast, the alloy density and the various magnetizations *(on a mass basis)* are sufficiently well known or well measured to be much less important in estimating the possible errors in f_h^v. Therefore, we can write

$$df_h^v = \frac{\partial f_h^v}{\partial \rho_b} \ d\rho_b + \frac{\partial f_h^v}{\partial \rho_c} \ d\rho_c$$

$$= \frac{\rho_c}{\rho_b} \ (1 - \frac{\sigma_c}{\sigma_a}) \ \frac{d\rho_b}{\rho_b} - \left[\frac{\rho_c}{\rho_b} \ (1 - \frac{\sigma_c}{\sigma_a}) + \frac{\rho_c}{\rho_a} \ \frac{\sigma_c}{\sigma_a} \right] \ \frac{d\rho_c}{\rho_c}$$

25
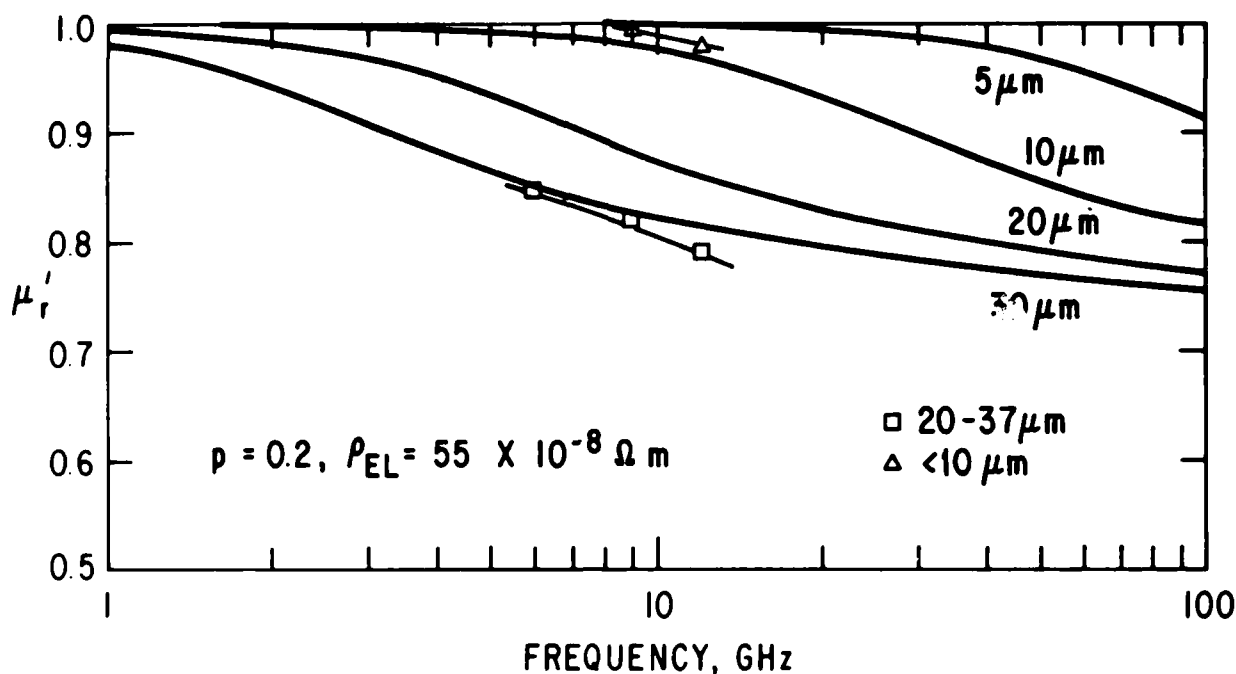
Figure 22. Comparison of Experiment and Model Calculations, $\mu_r{}'$ vs. f; p = 0.2.

When we substitute typical numbers into this formula we find: at the p = 0.4 level, a 2% error (uncertainty) in ρ_b contributes about 0.01 to df_h^v and a 1% error in ρ_c contributes a similar uncertainty (0.01) to df_h^v; at the p = 0.1 level each of such a pair of uncertainties (0.01) in df_h^v follows from 1% errors in ρ_b or ρ_c.

In Table 4 we present the result of the porosity calculation. Other characteristics of these samples such as volume loading and particle size were given in Table 3. The values of porosity are generally small. The scatter between positive and negative values (the latter are meaningless) say more about our uncertainties than about the composite samples. At this stage we conclude that the preparation method is sufficiently in control that porosity is not a significant factor for this set of samples to affect the electromagnetic parameters.

II.3.3 Direct Observation

Can we confirm the calculated conclusion that porosity in the polyurethane artificial dielectric composites is negligible? That would seem to be an easy task in these days when a scanning electron microscope (SEM) is often readily available. However, preparation of samples for observation is a special art which is needed in the case of these polymeric composites.

Our Polymer Physics Unit was able to help out with observations on these composites with special equipment. In the normal course of events, an as-cut sample was lightly coated with Au and Pd (a few hundred Angstroms coat) to carry off electronic charge and heat. However, if the sample was microtomed at room temperature, the resulting SEM picture was a mess, i.e., a torn surface which told more about the cut than about the composite. Their new equipment (an Ultracut E) allowed them to carry out a cold microtome at about -150C using a glass knife.

The SEM pictures shown in Figure 26 for one sample (ONR #2, p = 0.4, 20μm<d<37μm) are clean and interesting. There are faint but discernable circles which are cut(!) sections of the metal powder spheres. Their dimensions correspond to particle sizes used. Note that smaller sizes may be
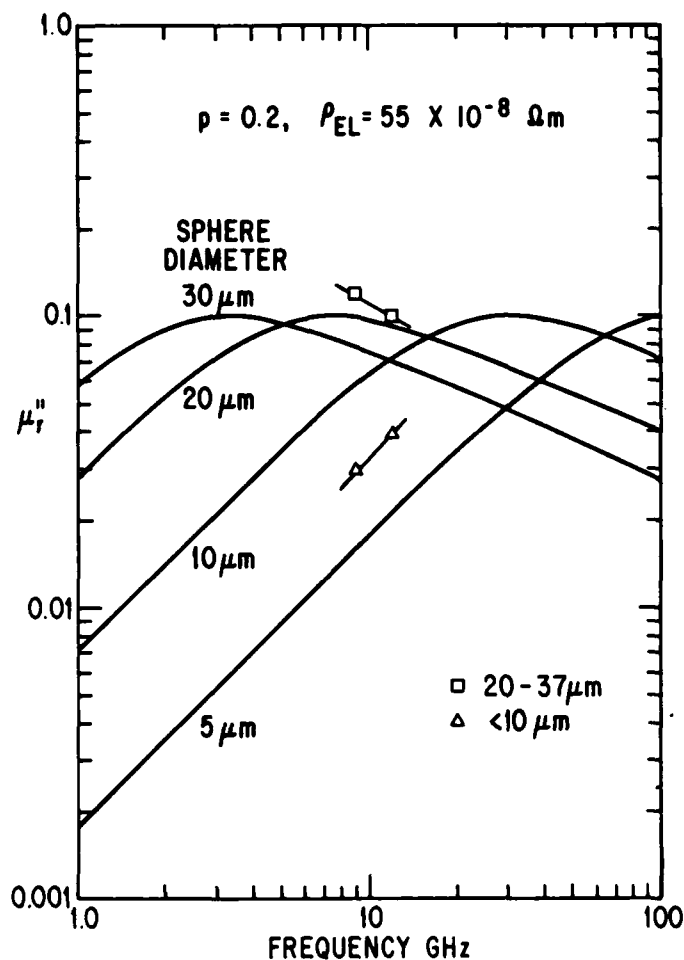
Figure 23. Comparison of Experiment and Model Calculations, μ_r'' vs. f; p = 0.2.

anticipated in the cut, and a few are distorted from the circular cross section. Their identity is confirmed by EDAX (Energy Dispersive Analysis by X-rays) which shows a high count for Ni and a lesser one for Cr on these circles in contrast to adjoining matrix. A number of holes are present. Some of these are *obviously* hemispherical "pull-outs." Others are distorted but with excess lip material suggesting a pull-out. There are many regions densely filled with material of one kind or another. The latter observation is in accord with the calculations suggesting negligible porosity. At this volume loading the metal particle density is sufficiently high that one cannot get a feel for "irregular fluctuations" in the loading.

It is a matter of concern for understanding the electromagnetic properties on a quantitative basis that one look for wide variations in local packing on some moderate length scale. Several workers have pointed out the potentially enormous effects that may arise from agglomeration with electric conduction contact [23] or wide variation in size distribution [24] intrinsically or as a consequence of agglomeration. In addition, as we discuss later herein, if a nominally dilute, low p-value composite has locally densely packed regions (of a size we hope to be able to investigate theoretically), compensated by regions nearly empty of metallic particles, *without* electric conduction paths in the densely packed regions, there can be some enhancement of electromagnetic property parameters. This arises from a strongly non-linear volume loading dependence of the property.
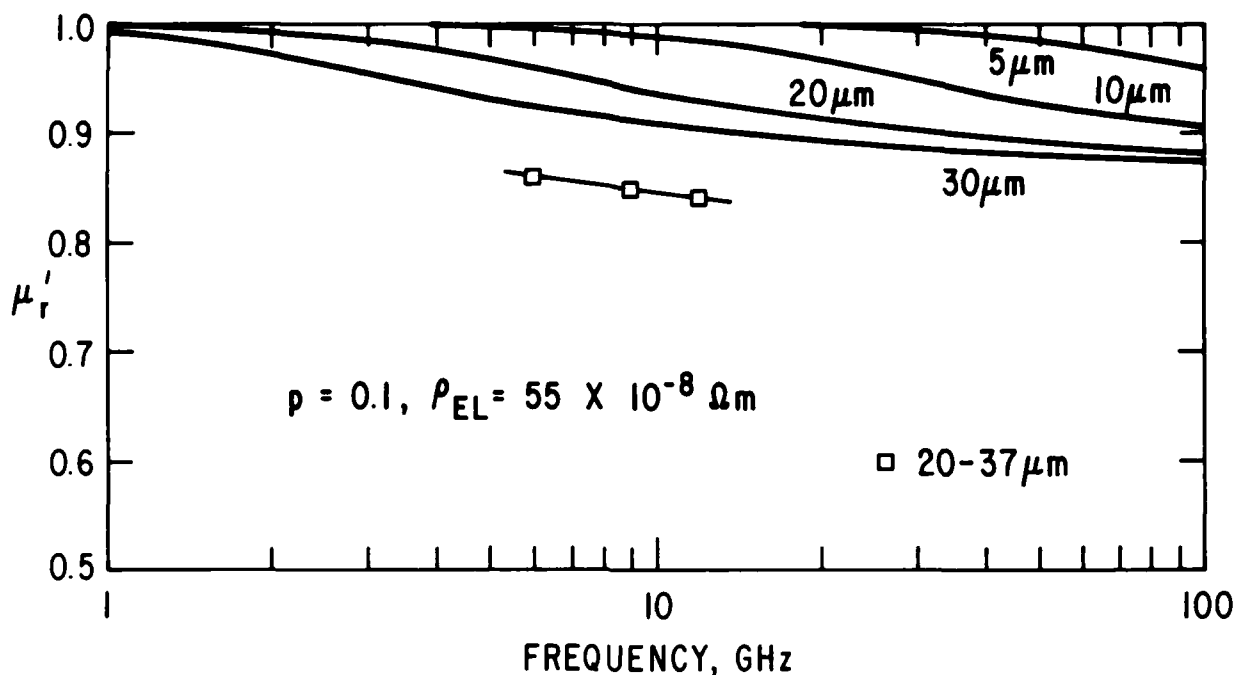
27

Figure 24. Comparison of Experiment and Model Calculations, μ_r' vs. f; p = 0.1.

We have not yet made direct observations on composites of lower p value, but we plan to examine the p = 0.1 sample (ONR #5) in the near future. Also under consideration is the preparation of composite samples with still lower p values, for electromagnetic measurement *and* direct (SEM) observation.

II.4 Alternative Theoretical Approaches to Composite Dielectrics

This section deals with an important task of the program. We have been quite successful in exploring a wide range of theoretical approaches from rather "classical" ones up to developments of the past half-dozen years, and in relating these to the materials physics of the applications of interest. This subject attracted much attention in the nineteenth century [2] and yet it remains quite alive today as evidenced by several recent topical conferences on the properties of heterogeneous media [18,25].

There is a basic distinction between several classes of models of such dielectric media. More modern theory follows the work of Bruggeman [2,26]. This is a symmetrical (two-component) effective medium model wherein particles of type 1 are mixed randomly in some proportion with those of type 2, so that each may be surrounded by particles of both types. If one type is conducting and the other insulating, there will be a percolation threshold composition at which conducting paths are established. The volume loading for this to occur is about 0.15 to 0.2. This model is often labeled EMA (eff. med. approx.).

In another (older) class of model one assumes that particles of type 1 are completely surrounded by material of type 2. It is clearly necessary to specify whether metal has been added to a dielectric host or vice versa, i.e., the model is unsymmetrical. This class of model is associated with the names of Maxwell, Maxwell-Garnett, Clausius and Mossotti, and Lorentz and Lorenz. It too is really an effective medium (or molecular field) model. It is variously called by any of the names just cited, e.g., MGT, CM, etc. Real-life examples of this model are ordered (cubical) arrays of spheres in a different medium, or an otherwise correlated medium such as coated spheres in a random arrangement, with each metal particle surrounded by a concentric dielectric coating. In our prior work [1] we employed this model (under the name Maxwell model) without a critical evaluation and with moderate success.

28
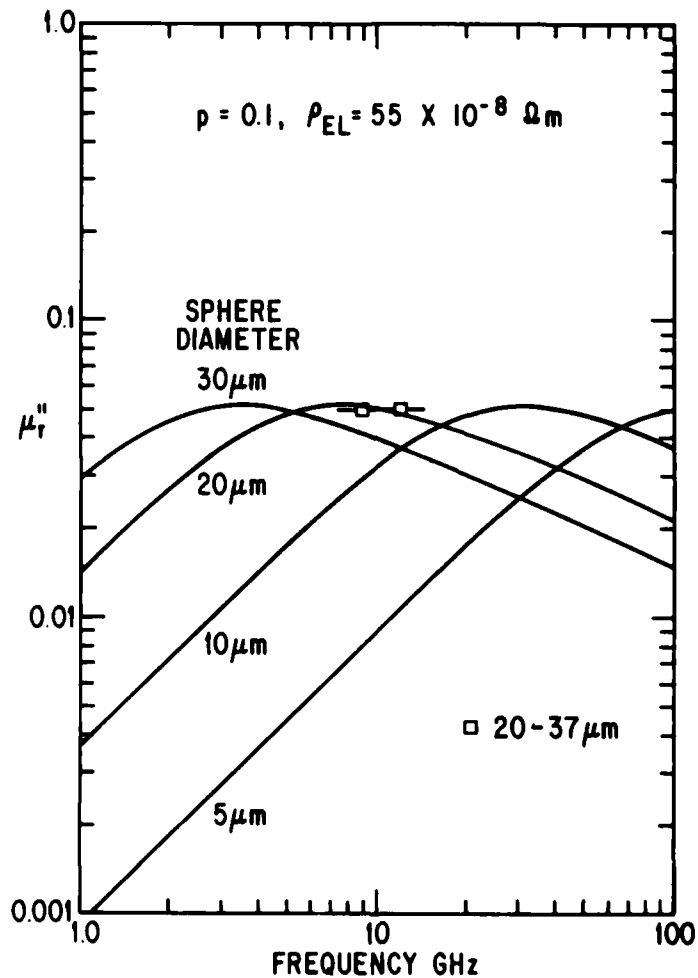
Figure 25. Comparison of Experiment and Model Calculations, μ_r'' vs. f; p = 0.1.

Table 4

CALCULATED POROSITIES
OF POLYURETHANE
TEST COUPONS

Sample #	f_h^v
2	+0.04
3	−0.05
4	−0.03
5	+0.01
6	−0.04
7	+0.07
8	+0.01

29

Figure 26. Scanning Electron Microscope views of cold-microtomed polymeric composite ONR #2 ($p = 0.4$, $20\mu m < d < 37\mu m$). Top photo at 150 x; lower photo at 500 x.

In recent years, rigorous calculations (and some measurements) of the *ordered* arrays have appeared [27,28,29,30] and they have relevance for the random *coated* array. Features of these theories are the significant effects of higher order multipoles beyond the dipole-dipole model and the (obvious, but sometimes ignored) maximum packing limits. Re-examination of the earlier data [1] confirm the applicability of these recent calculations, and deviations therefrom cast some light on the microstructure of the random coated arrays.

II.4.1 The Maxwell (MGT,CM) Model

An excellent derivation of the formulas for this model with emphasis on the concepts and approximations is presented by Landauer [2]. A contrasting experimentally oriented discussion on methods of approximating the behavior of two-phase (heterogeneous) systems has been developed by Mitoff [31].

Mitoff's report also calls attention to a very simple method described by Lichtenecker [32] for approximating the properties of two-phase systems, particularly when the properties of the two phases are not very different. Although the method is not fundamentally correct, it is easy to use and does agree with experimental results.

Lichtenecker's rule states that a plot of log k (k being the property value or "constant" for the composite) versus volume fraction p of phase 2 in phase 1 is a straight line between the end values. A graphical comparison with a correct treatment, such as Maxwell's (discussed below) shows that the difference between the two is insignificant with respect to experimental accuracy where the constants of the two phases are within an order of magnitude of each other.

Maxwell derived an equation which, at infinite dilution, exactly describes the k of a mixture of spheres with property constants k_1 and k_2, $(k_2 > k_1)$. While he used k_c and k_d for the continuous and the discontinuous phases, Mitoff recasts this into two expressions:

$$k = k_2 \left[\frac{k_1 + 2k_2 - 2(1-p)\ (k_2-k_1)}{k_1 + 2k_2 + (1-p)\ (k_2-k_1)} \right]$$

for phase 2 being the continuous phase; and

$$k = k_1 \left[\frac{k_2 + 2k_1 - 2p\ (k_1-k_2)}{k_2 + 2k_1 + p\ (k_1-k_2)} \right]$$

for phase 1 continuous. It assumes that the discontinuous phase consists of spheres and that the spheres are separated enough not to disturb the lines of "flux" around a neighbor. It has been shown by experiment to be quite accurate up to 10% dilution and is a fair approximation in *some* cases even up to 50%.

An alternative writing of the second of the above equations may be more familiar to some. Thus for the Maxwell, Maxwell-Garnett, Clausius-Mossotti model we also have

$$k = k_1 + \frac{3\ p\ k_1\ (k_2-k_1)}{(1-p)\ k_2 + (2+p)\ k_1}.$$

When $k_2 >> k_1$ and p is small (low-concentration) this formula reduces toward

$$k = k_1\ (1 + 3\ p).$$

Although equations of the general type above have been available for many years, they have seen little use, probably because they are not the kind one keeps in one's head for a quick approximation. Mitoff's report, however, shows that a very simple treatment applies when the two (separate) properties are very different. This is precisely the region for which the simple Lichtenecker method does not apply.

For large differences, extending to a number of orders of magnitude, one adopts the procedure of plotting log k/k_1 versus volume fraction. From Mitoff, we obtain Figure 27, presenting the Maxwell curves for k_2/k_1 ratios from $10^{0.3}$ to 10^6. The upper curves represent phase 2 continuous and the lower ones phase 1 continuous. The straight line, L, represents the Lichtenecker approximation. One notices that when k_2/k_1 is less than 10, the mathematically defensible Maxwell treatment is not much different from Lichtenecker's.

Mitoff goes a step further in observing that the limiting behaviors in Figure 27 for large differences $(k_2 >> k_1)$ are really straight lines with slopes that do not involve the property constant of the discontinuous phase. He obtains the relationships:

$$\frac{\Delta \log_{10} (k/k_2)}{\Delta (1-p)} \simeq -0.65 \quad (k_2 = k_c)$$

and

$$\frac{\Delta \log_{10} (k/k_1)}{\Delta p} \simeq 1.3 \quad (k_1 = k_c)$$

These are shown graphically on Figure 28. So long as the k's are very different, one expects the points to fall on these straight lines, especially at volume fractions close to the k_c side.
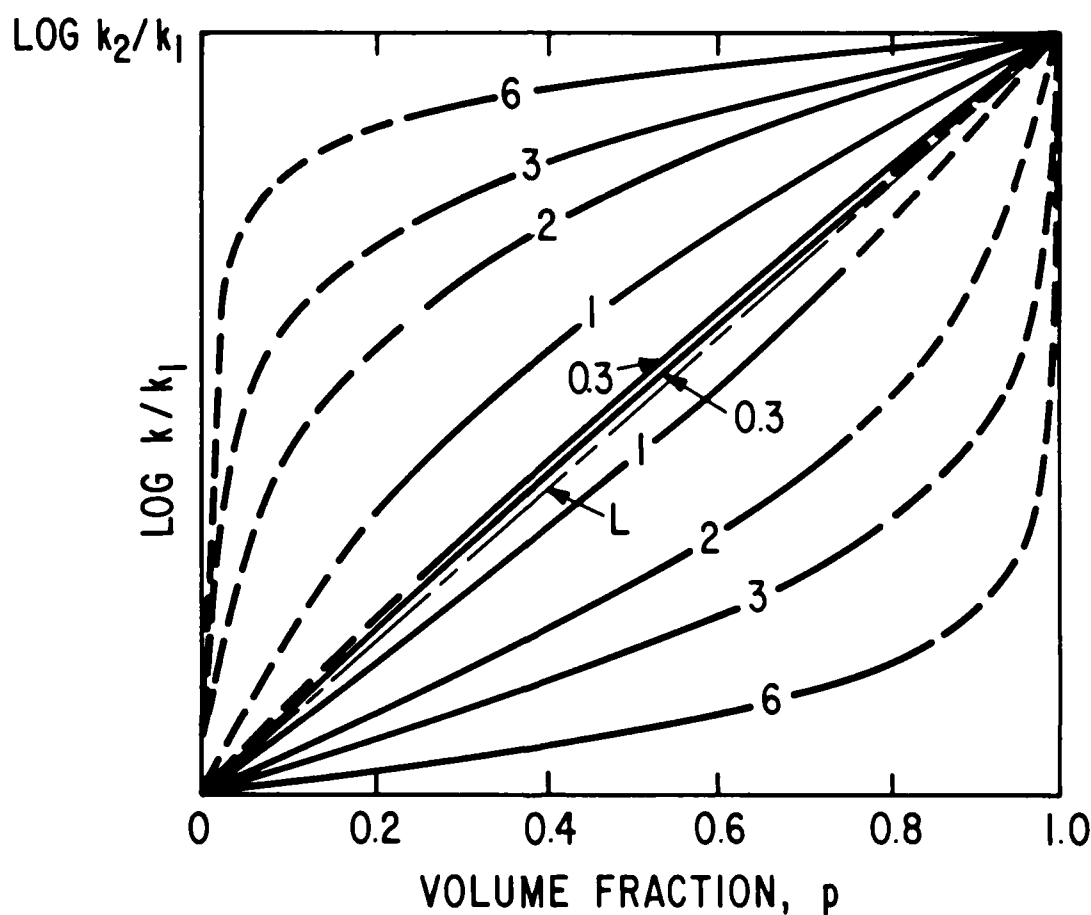

Figure 27.   Maxwell (MGT, CM) Equations for Mixtures, on a Semilog Plot. Upper set is for Phase 2 continuous; lower set is for Phase 1 continuous; L is Lichtenecker's Approximation. (The number on each curve signifies the power of ten in the ratio k_2/k_1.) (from Reference 31)
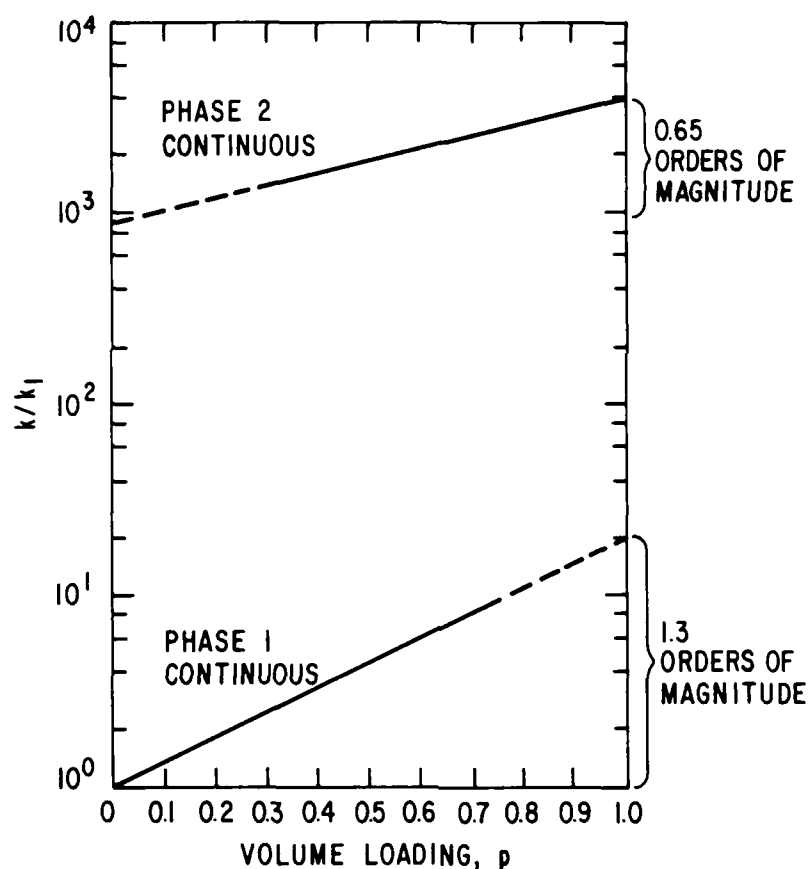
32

Figure 28. Mitoff's Graphical Approximations to the Maxwell (MGT, CM) Equations for $k_2 \gg k_1$. (from Reference 31)

Mitoff compares this approximate method with the complete Maxwell equation and with Lichtenecker's rule for a wide range of ratios of k_2/k_1. He shows that for one-order-of-magnitude difference or more the first or upper straight line for $k_2 = k_c$ is a fair approximation to Maxwell's result, and for two or more orders of magnitude difference the second or lower line for $k_1 = k_c$ is useful even out to rather high volume fractions of the discontinuous phase. At less than an order-of-magnitude difference, Lichtenecker's line is a good approximation to the Maxwell *equation* while the others are not.

Inspection of Figure 27 shows that the Maxwell (MGT, CM) expressions continue analytically across the whole range of volume fraction, p. That the curves are shown dashed at extreme p values is a recognition of two points: one is the assumption of non-contact, translated as meaning a dilute system; second is the fact that the volume loading of uniformly sized spheres in random packing cannot exceed 0.63, and reaches this only under specially favorable conditions. We return to this point below. Nevertheless the Maxwell (MGT, CM) formula is useful, as is the Mitoff approximation when used with care.

There are two applications of practical interest. The upper branch curves of Figure 27 (or their analytic expression) successfully describe the effects of porosity in a host medium. The second application of special interest is that of a coated sphere. Its relevance was noted in Section II.3.1. An apparently direct application of the Maxwell (MGT, CM) expressions yields [33] the single dielectric constant

$$\epsilon_{cs} = \epsilon_1 \left[\frac{2\epsilon_1 + \epsilon_2 + 2Q^3 (\epsilon_2 - \epsilon_1)}{2\epsilon_1 + \epsilon_2 - Q^3 (\epsilon_2 - \epsilon_1)} \right]$$

33

where

$$Q = 1 - (t/a)$$

with t the coating thickness and a the sphere radius. For $\epsilon_2 \gg \epsilon_1$, medium 1 being the insulating coat, this reduces to

$$\epsilon_{cs} = \epsilon_1 \left[\frac{1+2Q^3}{1-Q^3} \right].$$

For our estimated coating thickness of 0.1μm, on a sphere of average diameter 23μm, we find $\epsilon_{cs}/\epsilon_1 = 115$. For simplicity we take ϵ_1 for the coating as that for Cr_2O_3, i.e., 11.1, from which $\epsilon_{cs} = 1276$. This value for ϵ_{cs} is still so much greater than that for typical binders that the model calculations are unaffected.

II.4.2 The Bruggeman Effective Medium Approximation

We described the initial elements of this EMA model in II.4 above. A visual image is presented in Figure 29 (after Landauer [2]). The two components are mixed randomly. The shaded crystallite of type 1 (of volume fraction, p) is surrounded by crystallites of both types. In the analysis [2], the surrounding (two-phase) material is imagined as a single medium of uniform properties. The homogeneous dielectric constant ϵ_B in this case arises from the solution of a quadratic equation which, assuming spherical particles, is:

$$p \frac{\epsilon_B - \epsilon_1}{2\epsilon_B + \epsilon_1} + (1-p) \frac{\epsilon_B - \epsilon_2}{2\epsilon_B + \epsilon_2} = 0$$

At quite low concentrations, p, the EMA and the Maxwell-MGT-CM give identical results. The EMA has the appealing aspect of treating particles of types 1 and 2 on an equivalent basis (hence a symmetrical theory).
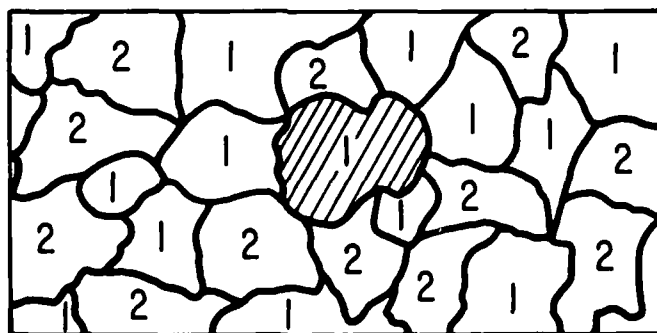

Figure 29.   Schematic View for Bruggeman Effective Medium Model. (from Reference 2)

34

As we have discussed above, our artificial dielectric is one with a correlation between the two phases of the medium. This rules against the use of the EMA model and in favor of one for which the metal is embedded in the insulating medium (thanks to the coating).

An interesting and distinctive feature of the EMA is that is predicts a metal-insulator or percolation transition. In this version it occurs at $p = 1/3$, while in other theories this value can be as low as $p = 0.15$. (For quasi-two-dimensional mixtures, the values are somewhat higher). A good illustration of this prediction *experimentally* is shown in Figure 30 [34]. For these samples the critical percolation fraction (vol. loading) is about 0.20. This demonstration is a convincing argument against the EMA class of model for the artificial dielectrics of this study.

II.4.3 Exact Calculations for Arrays of Spheres

Concurrent with the interest in random heterogeneous media, is an attention to the equivalent problem for *ordered* arrays of (conducting) elements. Lord Rayleigh in 1892 showed a significant advance beyond Maxwell's work when he took into account induced octupole moments. The ordered array lends itself to a more rigorous formulation of the problem. The subject received a technical boost with the suggestion of Kock [35] that artificial dielectrics (of the ordered type) could be used as microwave lenses. There has been a great deal of engineering interest, involving a variety of conductor shapes [36]. We have found particularly useful a paper by Kharadly and Jackson [27] both for the (lossless) effective permittivity calculations and measurements, and for discussions of the dielectric loss. Most recently, with modern computers, one can carry out numerical calculations of these problems to arbitrary precision limits which were totally unattainable heretofore [28-30,37,38].
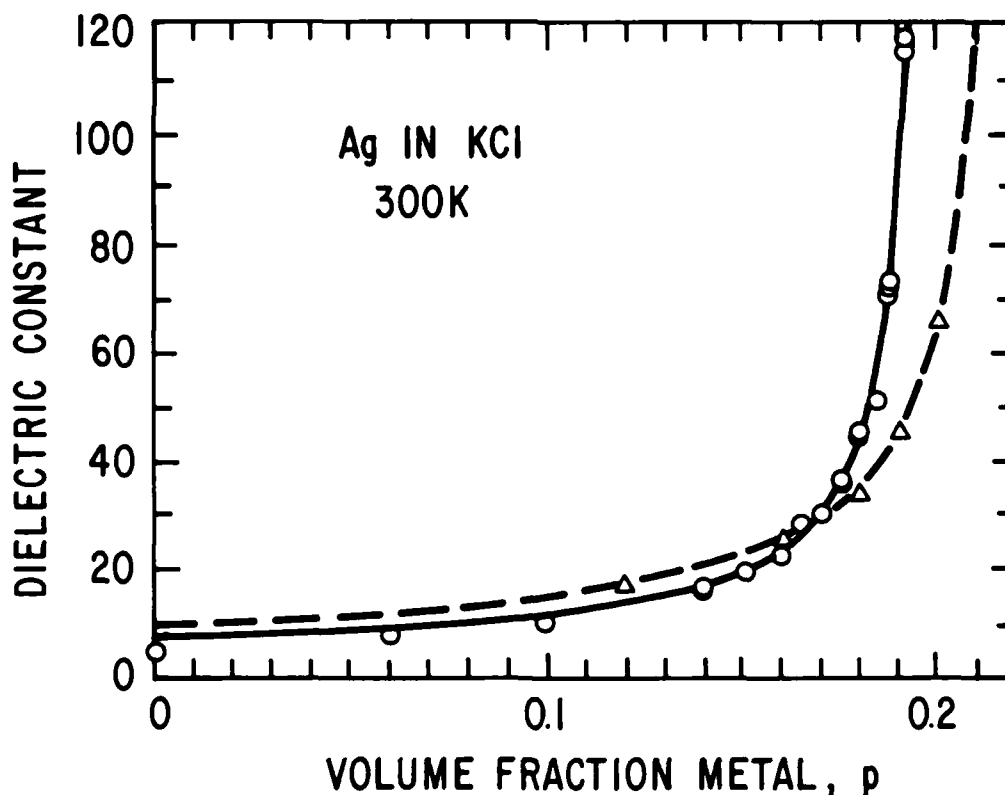

Figure 30. The Dielectric Constant of Several Ag-KCl Samples as a Function of Metal Volume Fraction, p. (from Reference 34)

35

As noted above, the higher order multipoles (beyond the dipole terms of the Maxwell/CM theories) have an important effect as the spherical conductors get closer at increased p. A measure of the success of the calculations is that the calculated permittivities exhibit an anomaly at the critical volume loading where the spheres just touch, in contrast with the Maxwell (MGT, CM) models. The conceptual drama of this feature shows in the simplicity of a confirmatory experiment for the body centered cubic lattice [30]. It suffices to construct only a one-eighth portion of a unit cell using conducting and insulating plates plus two one-eighth sections of metal ball bearings! The metal-insulator "anomaly" or transition when they touch is thus lattice dependent. This follows from the 3-dimensional packing limits for hard, uniform spheres, as follows:

simple cubic $p = \pi/6 = 0.52$

body centered cubic $p = \pi \sqrt{3}/8 = 0.68$

face centered cubic $p = \pi \sqrt{2}/6 = 0.74$
or hexagonal closed packed

In Figure 31 we reproduce the results of the calculations, the upper from Doyle [28,37] and the lower from the Australian group [29,30,38]. The Maxwell-CM curve in the upper portion agrees with the exact calculations out to $p \cong 0.35$ for SC and to $p \approx 0.5$ for BCC and FCC. This provides the justification for the reasonable success in our prior work. It was the right type of model and a not-bad approximation. On the other hand, the Maxwell/CM model fails to diverge until p tends toward unity. The line marked R is the Rayleigh calculation for the SC lattice (corrected [28]) showing some multipole effects but failing to diverge at the contact limit. In addition *experimental* data are included for the SC lattice which are in line with the exact results.

The calculations of the Australian group in the lower portion of Figure 31 agree in detail with those of Doyle, since the methods of attack were equivalent. They have added another curve estimated by *scaling arguments and intended to apply to a random or disordered array*. The *empirical* packing limit in this case (as noted above) is $p = 0.63$, although that limit is tricky to reach and values nearer to $p = 0.60$ are more likely. They even express this curve with a closed approximate formula as follows:

$$\epsilon = 0.05398 - 2.0675 \ln(0.63-p).$$

II.5 Dielectric Measurements and Analysis

In discussing the magnetic dipole effects (*induced*) in artificial dielectrics (Section II.2 above) it was important to examine both the real and imaginary parts of the permeability. Following the infrared studies of *small* metallic particles [17,19] it was noted that electric dipole effects contribute significantly to absorption in that frequency range only when the metal particle size is below about 50A. The size dependence of the magnetic dipole loss effect is one factor here. The other is that for appropriate models of the dielectric behavior of a metal [17,19,27] the frequency region for significant electric loss is governed by the intrinsic electron plasma frequency of the metal and the electron relaxation time. These correspond to frequencies in the ultraviolet and visible ranges, respectively, clearly far away from the microwave and millimeter frequency ranges of present interest.

Therefore, to the extent that we can consider our composite binders to approximate perfect (lossless) dielectrics, we need focus only on the real part, ϵ', in our measurements. From an operational point of view, however, we do not ignore the measurement results which include ϵ'' values. It is important to examine the measurement output for ϵ'' in that "unsmall values" are often a sign of erratic operation of the measurement process.

In what follows we shall revisit the dielectric behavior of composites included in our prior work with a view to reconciling this with the more modern theories. Finally we present and discuss the ϵ' data obtained on the composites prepared for this study.
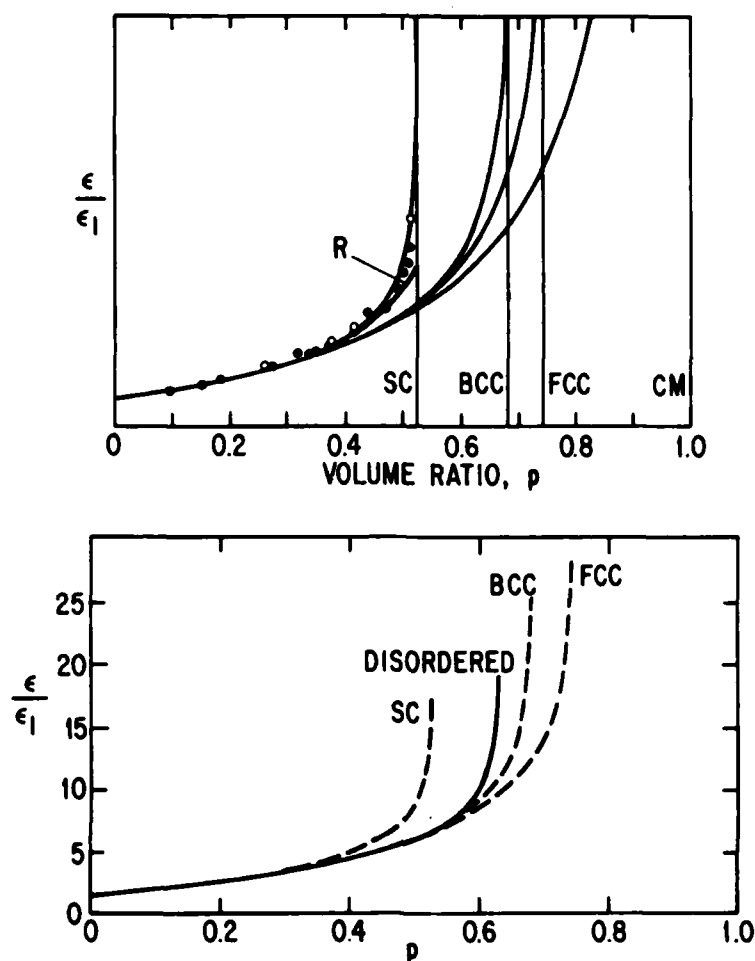
Figure 31. Dielectric Constants for Cubic Lattices as calculated in Ref. (28) (upper) and Refs. (29, 30) (lower).

II.5.1 Reanalysis of Prior ϵ' Results

In our prior study [1] we obtained dielectric measurement data on a composite system of magnetic metal particles in the same polyurethane binder as employed herein. The particles had an insulating coating (c.f. Section II.1.5.1 and Table 2). The composites studied had measured volume loading ranging from about $p = 0.25$ to $p = 0.50$. It is instructive to re-examine these data in the light of Section II.4, inasmuch as the prior analysis had considered only the Maxwell (MGT-CM) model.

In Figure 32 we display that ϵ' data set along with a number of comparative curves. The various symbols used for the data set refer to series with differing particle sizes and size ranges. Despite some experimental scatter, the family of data describe a general curve. The solid *straight line* passing through the lower p-value data is the Mitoff approximation to the Maxwell model. (Recall from Figure 28 that its slope is pre-determined.) In the limit of $p = 0$, this line comes close to, but deviates a bit from the ϵ' data point measured for the binder alone. We more-or-less ignored this deviation at the time of that work and we do not now have an explanation for it.
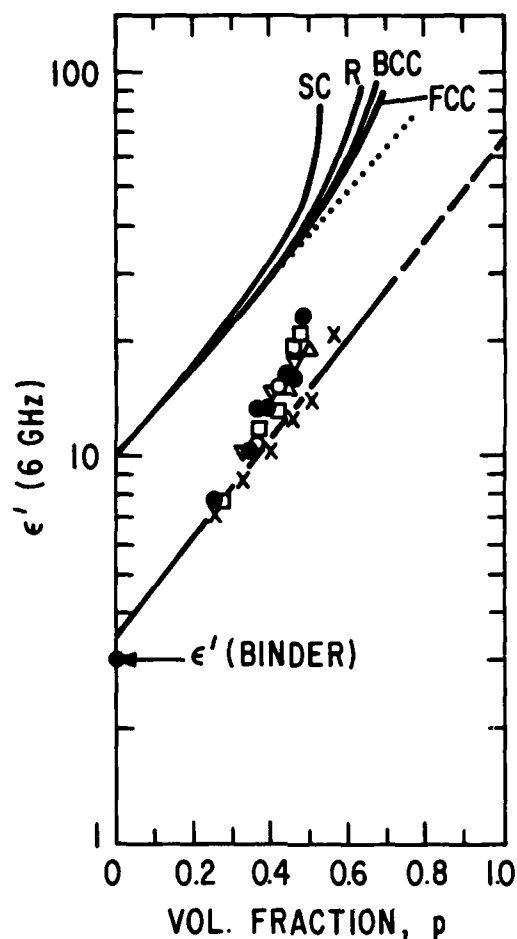
Figure 32. Measured Dielectric Constant Data from Prior Study; also Comparative Model Curves for Cubic Lattices (SC, BCC, FCC) and an Estimated Random Array Curve (R).

The upward deviation of the data from the Mitoff approximation line is a more prominent feature. In the prior study we tried to attribute the deviation to voids, without any analysis. That attempted explanation contradicts the effects of voids as we presently understand them. However, we do not have to look far for a qualitative explanation. The offset family of curves in Figure 32 are obtained from Figure 31, the calculated curves of ϵ' vs. p for cubic lattices, including higher order multipole effects. (The dotted curve is the Mitoff line, again). The general feature of the upward curvature of the ϵ' vs. p data is clearly a consequence of the multipole interations and the limits to packing.

From a quantitative point of view the explanation leaves room for comment. The data curve rises slightly more rapidly than the calculated curve for the simple cubic (SC) lattice. It is markedly away from the curve estimated for a random distribution. In discussions with Prof. W.T. Doyle of Dartmouth College (References 28, 37), he suggested an attractive explanation.

The suggestion is based on the marked non-linearity of the ϵ' vs. p curve. In contrast to the lattice arrays of particles, one could have fluctuations in volume loading in a randomly packed composite. Indeed fluctuations are the norm in random systems but we imagine that on some spatial scale it can make a difference. If, for example, a nominal p = 0.50 sample were comprised of equal parts of p = 0.4 and p = 0.6 loadings, the ratio ϵ/ϵ_1 would be 5.20 instead of the estimated random ratio of 4.27. (The separate values of ϵ/ϵ_1 for p = 0.4, 0.6 are taken from the estimated curve/formula in Section II.4.3).

38

We remarked on this aspect of the random composites in Section II.3.3 in connection with direct observation of the composite in a SEM. For the one $p = 0.4$ sample shown in Figure 26, such effects are not easily detected. By examining some more dilute samples we hope to find evidence for such (non-contacting) clumping.

In addition there may be some interesting questions about the spatial scale of clumping needed to produce the electromagnetic effects hypothesized. We plan to pursue these and related points in a collaboration/consultation with Professor Doyle.

II.5.2 Measurements on Non-Magnetic Composites

The artificial dielectric composite samples described in Section II.1.6 were measured by the techniques of Section II.2.4. Major emphasis at this stage has been on the frequency range 6-12 GHz. Extensions to lower and higher frequencies are underway, including measurement at 35 GHz. Future plans call for measurements at 94 GHz. (Permeability results on these samples were reported in Section II.2.4.1). In Figure 33, we show examples of these measurements for 3 samples, $p = 0.4, 0.3,$ 0.2 of the $Ni_{92}Cr_8$ powder in polyurethane with $20\mu m < d < 37\mu m$. (Samples ONR #2, #3, #4).

An overview of the ϵ' vs. p data is presented in Figure 34, along with a few model curves. Of the latter, it is useful to see how closely the Mitoff approximation line comes to matching the exact simple cubic array dielectric curve. In considering the measured data, picked at 10.5 GHz where the noise is minimal, it is clear that we have a problem. The data could be fit reasonably with a Mitoff line, but only if we ignore the binder-only point (taken anew for this study).
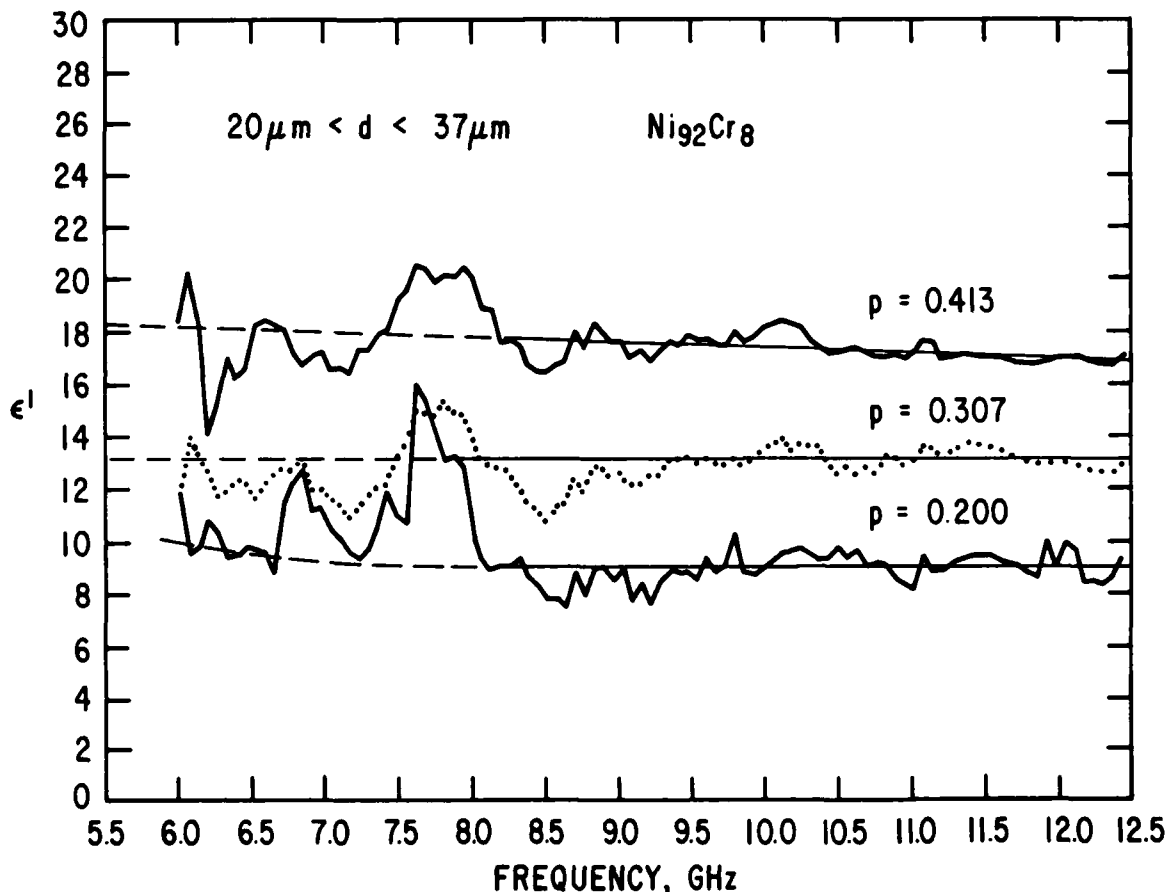

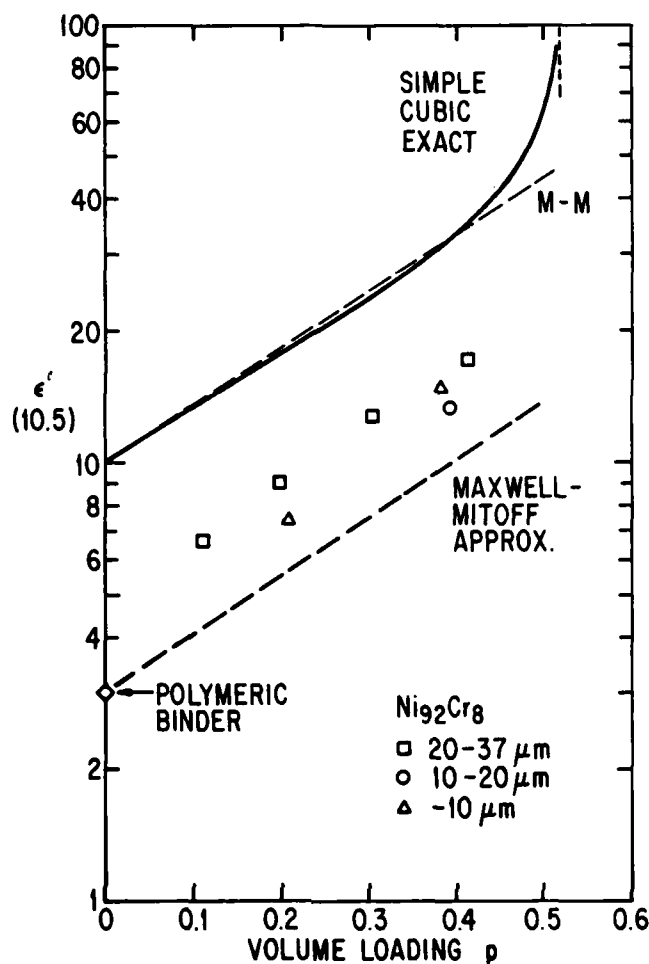Figure 33. Relative Real Permittivity, ϵ_r', vs. Frequency; Range 6-12 GHz. Samples ONR #2, 3, 4.

39

Figure 34. Overview of Relative Permittivity, ϵ' vs. p Various particle sizes; $Ni_{92}Cr_8$ in Polyurethane Composites.

It seems rather far to stretch to attribute this upward shift to clumping in the way just described (See II.5.1). At this stage, with limited data, there does not seem to be any significant variation with particle size. We would not expect any under ideal conditions.

We shall continue this investigation in depth in order to resolve the problem. We plan to make (by the same techniques) samples with lower p-values. The independent measurements currently underway at 35GHz may confirm or deny the accuracy of the techniques used. It is additionally puzzling that the prior data shown in Figure 32 exhibited this effect so modestly that we tended to ignore it.

This concludes our report on the group of Tasks numbered 1, 2 and 3 in Table 1.

III. TASK 5: EXPLORE ALTERNATIVE PASSIVATION COATINGS

The system of interest in the prior work [1] has been called an oxide- passivated metal-insulator dielectric. The oxide coating was obtained by a classified technique. In the present study, scheduled for the second year, there is a task of exploring alternative or improved coatings. We have made a start on this task and details are presented in a classified appendix to this Annual Report.

IV. TASK 6: QUANTIFY SKIN-DEPTH EFFECTS IN PASSIVATED ARTIFICIAL DIELECTRICS

From our paraphrasing of the Statement of Work, this task can be posed under the question -- Has the artificial (magneto-) dielectric system been optimized in the centimeter wavelength regime? Achieving such a goal carries with it the possibility of predicting the particle sizes needed for millimeter wavelength applications.

It was our intent to conduct this portion largely empirically, and then deduce the guiding rules which would facilitate prediction. There is however, some reason to feel that a reasonably analytic approach may be possible, in parallel with the experiments.

The main challenge in this task is in the area of *fine metal powder preparation, and processing*.

IV.1 Spark Erosion Preparation of Fine Powders

We have made a promising start toward the preparation of powders for high-frequency optimization of the artificial magneto-dielectric system. We are exploiting the potential of the spark erosion technique to prepare suitable crystalline alloy particles. This technique has enjoyed renewed attention of late with important contributions from our colleagues.

A schematic of the spark erosion apparatus is shown in Figure 35. The process of spark erosion [39] results from maintaining a repetitive pulsed spark discharge between electrodes immersed in a dielectric fluid. The spark discharge produces highly localized superheated regions in the electrodes. Small molten droplets and vaporized materials are ejected from these heated regions into the dielectric fluid, where they are rapidly cooled into particles. This process was used to prepare colloids at least 50 years ago. In more recent times it is the basis of electric discharge machining. The choice of dielectric fluids can range from organics through aqueous and cryogenic liquids.
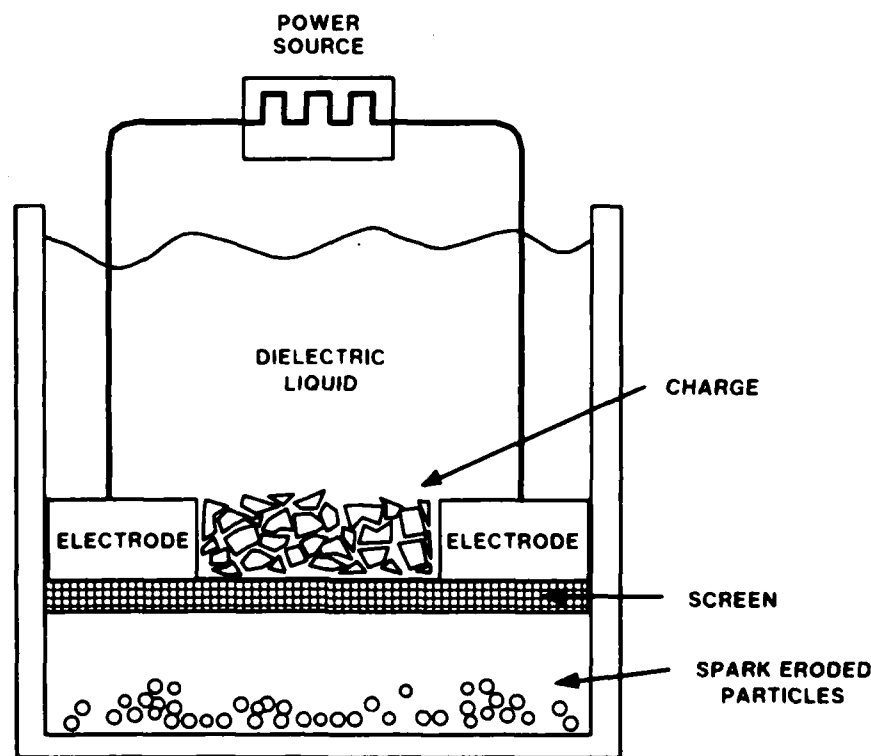

Figure 35. Spark Erosion Apparatus. The electrodes and the coarse charge are of the same composition. The larger particles ($>0.5\mu$m) which form from erosion of the charge and electrodes settle through the screen.

Previous workers have noted that the particle yield could have a bimodal distribution of diameters. Smaller particles with average diameters about 50A tend to remain in colloidal dispersion. "Larger" particles, with diameters between 0.5 and 25μm, settle out. Our colleagues have recently examined the smaller ones with a view toward their application as metallic ferrofluid particles (instead of the usual magnetite, Fe_3O_4, ferrofluid material) [39].

In the present work our immediate goal is to prepare and separate powders, and then evaluate composites of magnetic alloy particles in the less than 1μ range. This will be a continuation of prior work which studied artificial dielectric material of various particle sizes down to a range of 1 to 4μm diameter in an insulating binder [1]. Secondarily this task addresses the question of just how effective the spark erosion method might be as an alternative for general fine powder alloy production.

A large number of experiments have been undertaken using electrodes and charge of several suitable alloys. The dielectric fluids have included liquid argon, liquid nitrogen, ethyl-alcohol, water and, most recently, mixtures of the last two. Another significant variable in these tests is the duration of the spark pulse, e.g., short at 3μs and long at 50μs.

With the aqueous fluids, there is a distinct tendency for the particle size distribution to shift toward smaller particles with shorter spark discharge pulses. There have been major ($>50\%$) yields in the $d<10\mu$m range. This is extremely interesting when compared with existing commercial techniques.

The technological potential inherent in cheap dielectric fluids, such as water or water-based mixtures, is also very attractive. It permits a freer rein in design conception when one considers possible scale-up.

On the other hand there is a greater tendency for oxidative processes to accompany the particle formation in an aqueous fluid. We are just beginning to sort out these effects and hence a discussion of detailed results will be deferred to a future report.

IV.2 Possible Analytic Approach to Skin-Depth Effects in Artificial Dielectrics

The goals of optimizing the system (i.e., the metal particle size) in the centimeter wavelength range and forecasting the properties at higher frequencies were posed originally as semi-empirical tasks. The progress reported in Section II.2. on understanding and demonstrating induced magnetic dipole and particle size effects has changed our view of the possibilities. The development at that point was for a strictly non-magnetic artificial dielectric. The present task carries the implied goal of involving the magneto-dielectric system of our prior study [1].

In that earlier work we examined, in a very simple model, some eddy current screening effects on the intrinsic magnetic permeability (μ', μ''). We did not however, incorporate this into a global model. In the course of the present work we encountered an old study which presents an overall attack on frequency dependence of such heterogeneous systems. On the other hand, it omits the ferromagnetic resonance considerations which formed an important part of our prior study. We feel that there is an interesting potential here in revisiting that older work and marrying it to the additional concepts just noted. We take this as a supplementary goal in the coming period of investigation.

V. CONCLUSIONS AND FUTURE PLANS

Inasmuch as we are just one-third of the way into this extended study, the matter of "conclusions" is only partly that, and partly an accounting of achievements en route to goals. It is thus appropriate to follow such a status review with an enumeration of plans for the coming period.

V.1 Conclusions

During the first phase of the study we have developed an interesting artificial dielectric. It is comprised of spherical alloy powder particles of the composition $Ni_{92}Cr_8$ prepared by gas atomization

42

with liquid substrate quenching which produces an insulating oxide coating on each particle. The composites fabricated with the metal powder and polyurethane are ferromagnetic only below room temperature, a feature which allows for easy determination of volume loading. Before mixing with the binder, the particles are classified by size at $<10\mu$m, $+10-20\mu$m, and $+20-37\mu$m.

The decision to pay close attention to powder size followed from the realization that examination of induced magnetic dipole (eddy current) effects would be as important as the dielectric studies originally planned. Calculations of complex magnetic permeability, adapted from the literature, showed that the dominant parameter is the ratio of particle radius to skin depth. The sizes chosen and frequencies of study (centimeter to millimeter wavelength ranges) cover the most interesting behavior anticipated. Measurements so far, mainly in the 6-12 GHz band, agree with calculations within about 20%. The results have applications consequences for understanding the properties of metallic magneto-dielectrics under extreme conditions of temperature or frequency, as well as for their frequency dependence under "normal" operating conditions.

Exploration of theoretical developments in the dielectric behavior of heterogeneous media has successfully addressed one of our opening questions, i.e., why our prior (and present) material systems follow so well the simple Maxwell (Maxwell-Garnett, Clausius and Mossotti) theoretical model. The inherently isolated metallic particles represent a correlated system even when loaded randomly in a binder, in contrast to the percolation-prone Bruggeman model exemplified in many experimental metal-insulator composites. Modern theories which incorporate higher order electric multipole effects and geometrical packing limits have been validated previously only (to our knowledge) by ordered lattice-like arrays of spherical particles. Our random composites also exhibit such properties, albeit with deviations probably reflecting on their microstructure.

We started work on alternative passivation coatings, of interest scientifically and technologically. We have also made good progress toward the preparation of very fine powders by the spark erosion method, with the goal of an empirical optimization of the metallic magneto-dielectric system in the centimeter wavelength range. The initial results on particle size *distribution* are quite interesting with future technological potential. The use of simple dielectric fluids including aqueous mixtures or water alone also holds technological promise.

V.2 Future Plans

We are quite interested in exploiting possible relationships between our combined experimental and theoretical success with the complex permeability of the non-magnetic artificial composites and the recent decade of results and calculations on anomalous absorption in the far infrared by fine metal particle composites. The anomalies of the latter studies represent a disagreement between theory and experiment of several orders of magnitude, in contrast to our reasonable success. To be sure, our frequencies and sizes differ from those of the infra-red studies by about a factor of ten (each) but that is not so far away considering the contrasting behaviors. We hope to investigate the connections, and perhaps to explore the possibility of collaboration with one of the academic groups working in the infra-red. Essential to this is some extension of our own work into the millimeter wavelength range, a task which is a bit behind schedule, in part because of changes in scope.

The dielectric property phase of the study holds several interesting challenges. One is to explore experimentally the possible clustering in randomly packed composites toward understanding the deviations in the ϵ' vs. p behavior. Some theoretical approaches to dielectric properties as related to the dimensions of fluctuations in packing may be undertaken. We hope to work with Prof. W.T. Doyle of Dartmouth on this aspect. Perhaps related to these aspects is the problem of apparently poor correlation in our new artificial dielectric system between the trend of ϵ' vs. p and the p = 0 limit (binder only) measured value. We need to understand this discrepancy.

Another problem area is the fabrication of a composite system using a second binder of noticeably different ϵ'.

We intend to pursue the alternative coatings investigations as outlined.

43

There is some excitement in the future as regards the goal of optimizing the magneto-dielectric system in the centimeter wavelength range and predicting the properties in the millimeter range. Experimentally this excitement centers on the research and technology potentials associated with fine powder production by the spark erosion method. Analytically we are cautiously hopeful that our progress in understanding the induced magnetic dipole effects can be extended and broadened to be a quantitative predictive tool for metallic magneto-dielectric systems. We plan to push this as well.

VI. ACKNOWLEDGEMENTS

REFERENCES

[1] I.S. Jacobs, H. Kirtchik, J.M. McGrath and R.N. Silz, "Magnetic RAM Technology - Phase II (U)," AFWAL-TR-82-1040, Final Technical Report for Contract F33615-80-C-1040, General Electric Company, Sept. 1982, SECRET.

[2] R. Landauer, "Electrical Conductivity in Inhomogeneous Media," in *Electrical Transport and Optical Properties of Inhomogeneous Media*, edited by J.C. Garland and D.B. Tanner, AIP Conference Proceedings No. 40 (1978), pp. 2-45.

[3] K.D. Cummings, J.C. Garland and D.B. Turner, "Electromagnetic Propagation in Random Composite Materials," in *Physics and Chemistry of Porous Media*, ed. by D.L. Johnson and P.N. Sen, AIP Conf. Proc. No. 107, (1984), pp. 38-51.

[4] S.A. Miller, "Amorphous Metal Powder, Production and Consolidation," in *Amorphous Metallic Alloys*, ed. by F.E. Luborsky, (Butterworth, London, 1983), pp. 506-519; S.A. Miller and R.J. Murphy "A Gas-Water Atomization Process for Producing Amorphous Powders," Scripta Met. *13*, 673 (1979).

[5] (Ni-Cr): R.M. Bozorth, *Ferromagnetism*, (D. Van Nostrand, New York, 1951), pp. 307-8; M. Hansen, *Constitution of Binary Alloys*, (McGraw-Hill, New York, 1958), pp. 541-6; K. Hoselitz, *Ferromagnetic Properties of Metals and Alloys*, (Oxford University Press, London, 1952), p. 302.

[6] (Gd-Y): W.C. Thoburn, S. Legvold and F.H. Spedding, "Magnetic Properties of the Gd-La and Gd-Y Alloys," Phys. Rev. *110*, 1298-1301 (1958).

[7] I. Cosma, I. Lupsa, O. Pop and M. Vancea, "Paramagnetic Properties of Ni-Cu-Al Alloys," Physics Lett. *49A*, 87-88 (1974); W. Köster, U. Zwicker and K. Moeller, "Mikroskopische und röntgenographische Untersuchungen zur Kenntnis des Systems Kupfer-Nickel-Aluminium," Zeits. Metallkunde *39*, 225-231 (1948).

[8] V. Marian, "Les points de Curie ferromagnétiques et la saturation absolue de quelques alliages de nickel," Annales de Physique, Ser. II, *7*, 459-527 (1937).

[9] C. Sadron, "Sur le ferromagnétisme des alliages de nickel et de chrome," Compt. rend. Acad. Sci. *190*, 1339-40 (1930).

[10] J. Šafránek, "Aimantation des alliages nickel-chrome au-dessus du point de Curie," Revue de Métallurgie (Memoires) *21*, 86-111 (1924).

[11] H.C. Van Elst, B. Lubach and G.J. Van den Berg, "The Magnetization of Some Nickel Alloys in Magnetic Fields up to 15 kOe between 0K and 300K," Physica *28*, 1297-1317 (1962).

[12] M.J. Besnus, Y. Gottehrer and G. Munschy, "Magnetic Properties of Ni-Cr Alloys," Phys. Stat. Sol. (b) *49*, 597-607 (1972).

[13] H. Tange, T. Yonei and M. Goto, "Forced Volume Magnetostriction of Ni-Cr Alloys," J. Phys. Soc. Japan *50*, 454-460 (1981).

[14] M.A. Simpson and T.F. Smith, "Thermodynamic Studies and Magnetic Ordering of Ni-Cr Alloys Close to the Critical Composition," Aust. J. Phys. *35*, 307-19 (1982).

[15] K. Hauffe, *Oxidation of Metals*, (Plenum Press, New York, 1965), p. 184, Fig. 73.

[16] H. Ottavi, J. Clerc, G. Giraud, J. Roussenq, E. Guyon and C.D. Mitescu, "Electrical Conductivity of a Mixture of Conducting and Insulating Spheres: an Application of Some Percolation Concepts," J. Phys. C: Solid State, *11*, 1311-28 (1978).

[17] D.B. Tanner, A.J. Sievers and R.A. Buhrman, "Far-infrared Absorption in Small Metallic Particles" Phys. Rev. *B 11*, 1330-1341 (1975).

[18] A large number of articles and references may be found in *Electrical Transport and Optical Properties of Inhomogeneous Media*, edited by J.C. Garland and D.B. Tanner, AIP Conference Proceedings, No. 40 (American Institute of Physics, New York, 1978).

[19] N.E. Russell, J.C. Garland and D.B. Tanner, "Absorption of Far-infrared Radiation by Random Metal Composites," Phys. Rev. *B23*, 632-9 (1981).

[20] L.D. Landau and E.M. Lifshitz, *Electrodynamics of Continuous Media* (Addison-Wesley, Reading, Mass. - Pergamon Press, New York, 1960), pp. 192-4.

[21] H. Thomas, "Über Widerstandslegierungen," Zeits. Physik *129*, 219-232 (1951).

[22] W. Heister, "Untersuchung der Frequenz-abhängigkeit der Stoffwerte ferromagnetischer Mischkörper bis zu sehr hohen Frequenzen," Archiv. f. Elektrotechnik *41*, 142-160 (1953).

[23] R.P. Devaty and A.J. Sievers, "Far-Infrared Absorption by Small Metal Particles," Phys. Rev. Lett. *52*, 1344-47 (1984).

[24] P. Chýlek, D. Boice and R.G. Pinnick, "Far-Infrared Absorption of Small-Palladium-Particle Composites," Phys. Rev. *B27*, 5107-9 (1983).

[25] *Physics and Chemistry of Porous Media*, edited by D.L. Johnson and P.N. Sen, AIP Conference Proceedings, No. 107 (American Institute of Physics, New York, 1984).

[26] D.A.G. Bruggeman, "Berechnung verschiedener physikalische Konstanten von heterogenen Substanzen, I., Dielektrizitätskonstanten und Leitfähigkeiten der Mischkörper aus isotropen Substanzen," Ann. Phys. (Leipzig) [5], *24*, 636-679 (1935).

[27] M.M. Z. Kharadly and W. Jackson, "The Properties of Artificial Dielectrics Comprising Arrays of Conducting Elements," Proc. Inst. Elec. Eng. *100*, Part 3, 199-212 (1953).

[28] W.T. Doyle, "The Clausius-Mossotti Problem for Cubic Arrays of Spheres," J. Appl. Phys. *49* 795-797 (1978).

[29] R.C. McPhedran and D.R. McKenzie, "The Conductivity of Lattices of Spheres. I. The Simple Cubic Lattice," Proc. Roy Soc. Lond. *A359*, 45-63 (1978).

[30] D.R. McKenzie, R.C. McPhedran and G.H. Derrick, "The Conductivity of Lattices of Spheres. II. The Body Centred and Face Centred Cubic Lattices," Proc. Roy. Soc. Lond. *A362*, 211-232 (1978).

[31] S.P. Mitoff, "Properties Calculations for Heterogeneous Systems" in *Advances in Materials Research*, edited by H. Herman, (Interscience- John Wiley, New York, 1968) vol. 3, pp. 305-329.

[32] K. Lichtenecker, "Die Dielektrizitäts-konstante natürlicher und kunstlicher Mischkörper," Physik. Zeits. *27*, 115-158 (1926).

[33] The standard reference at this point is H.C. van de Hulst, *Light Scattering by Small Particles*, (John Wiley, New York, 1975), but it is not easy to find the equation of interest. Therefore see W. Lamb, D.M. Wood and N.W. Ashcroft, "Optical Properties and Small Particle Composites: Theories and Applications" in *Electrical Transport and Optical Properties of Inhomogeneous Media*, ed. by J.C. Garland and D.B. Tanner, AIP Conference Proceedings No. 40 (1978), pp. 240-254, esp. eqs. 16, 17.

[34] D.M. Grannan, J.C Garland and D.B. Tanner, "Critical Behavior of the Dielectric Constant of a Random Composite near the Percolation Threshold" Phys. Rev. Lett. *46*, 375-378 (1981).

[35] W.E. Kock, "Metallic Delay Lenses," Bell System Technical Journal *27*, 58-82 (1948).

[36] R.E. Collin, *Field Theory of Guided Waves*, (McGraw-Hill, New York, 1960), Ch. 12 "Artificial Dielectrics," pp. 509-551.

[37] W. T. Doyle, "The Permittivity of Cubic Arrays of Spheres" in *Electrical Transport and Optical Properties of Inhomogeneous Media*, ed. by J.C. Garland and D.B. Tanner, AIP Conference Proceedings No. 40 (1978), pp. 300-304.

[38] R.C. McPhedran and D.R. McKenzie, "Exact Solutions for Transport Properties of Arrays of Spheres," ibid. pp. 294-299.

[39] A.E. Berkowitz and J.L. Walter, "Amorphous Particles Produced by Spark Erosion," Materials Science and Engineering, *55*, 275-287 (1982); "Ferrofluids Prepared by Spark Erosion," Jnl. Magnetism and Magnetic Materials, *39*, 75-78 (1983).

END

FILMED

2-85

DTIC